Mobility & Vehicle Mechanics

International Journal for Vehicle Mechanics, Engines and Transportation Systems

M V M   Mobility Vehicle Mechanics

Mobility & Motorna

Volume 50
Vehicle Number 1 Vozila i
2024.

Mechanics Motori

INDUSTRIAL WHEELS FOR INTERNAL TRANSPORT EQUIPMENT IN AUTOMOTIVE INDUSTRY

Nenad Miloradović [1], Rodoljub Vujanac [2]*

ABSTRACT: During many transport manipulative operations within the automotive industry, the supporting structure of the used equipment relies on various industrial wheels. The paper describes the characteristic types of wheels and castors and their constituent components. The role of the wheels with rubber and polyurethane coatings and with hard tread is highlighted. The process of choosing the right wheel for the given working conditions is presented. In addition to numerous applications in automotive and mechanical industries, various types of the wheels are also used on: machinery and equipment for the food industry, packaging and transport containers, constructions, scaffolding and road paving equipment, hospital equipment, environmental installations, entertainment equipment and as components in the textile and furniture industry or the sports equipment. Examples of concrete solutions for transport systems within logistic and manipulative operations are given.

[1] *Nenad Miloradović, University of Kragujevac, Faculty of Engineering, 6 Sestre Janjić Str., 34000 Kragujevac, Serbia, mnenad@kg.ac.rs , https://orcid.org/0000-0001-6846-6091*
[2] *Rodoljub Vujanac, University of Kragujevac, Faculty of Engineering, 6 Sestre Janjić Str., 34000 Kragujevac, Serbia, vujanac@kg.ac.rs , https://orcid.org/0000-0002-8215-5668 (*Corresponding author)*

INDUSTRIJSKI TOČKOVI ZA SREDSTVA UNUTRAŠNJEG TRANSPORTA U AUTOMOBILSKOJ INDUSTRIJI

REZIME: Tokom mnogih transportno manipulativnih operacija u okviru automobilske industrije, noseća konstrukcija korišćene opreme se oslanja na različite industrijske točkove. U radu su opisani karakteristični tipovi točkova i nosača, kao i njihove sastavne komponente. Istaknuta je uloga točkova sa gumenom i poliuretanskom oblogom, kao i sa tvrdim gazećim slojem. Prikazan je proces izbora pravog točka za zadate radne uslove. Pored brojnih primena u automobilskoj i mašinskoj industriji, razne vrste točkova se takođe koriste u: mašinama i opremi za prehrambenu industriju, ambalaži i transportnim kontejnerima, u građevinarstvu, na skelama i asfaltiranju puteva, bolničkoj opremi, ekološkim instalacijama, opremi za zabavu, kao komponenta u tekstilnoj industriji i industriji nameštaja ili kao element sportske opreme. Navedeni su primeri konkretnih rešenja transportnih sistema u okviru logističkih i manipulativnih operacija.

KLJUČNE REČI: *industrijski točkovi, automobilska industrija, unutrašnji transport*

INDUSTRIAL WHEELS FOR INTERNAL TRANSPORT EQUIPMENT IN AUTOMOTIVE INDUSTRY

Nenad Miloradović, Rodoljub Vujanac

INTRODUCTION

Internal transport is an important part of material handling in all types of the production processes. Related methods of internal transport should be cost-effective, low energy consuming, safe, smooth and quiet. They should also help to increase productivity and profitability of the industrial processes. Many operations are part of the internal transport (loading, unloading, reloading and transfer). The scope of internal transport operations includes various mechanical, hydraulic, pneumatic and electrical systems, with autonomous systems as modern additions [1].

Internal transport devices use industrial wheels and brackets during transportation and manipulative processes in various applications. Each application involves specific operating conditions that are defined by technical solutions and international standards. Various types of industrial wheels are in use [2], like the wheels with rubber, polyurethane, monolithic (hard tread) and pneumatic coverings.

The tyred wheels have coverings made of elastomer that originates from natural and/or synthesised rubber and is made by using vulcanization or injection moulding. During the vulcanization process and due to added mineral agents, rubber acquires improved elastic properties over time that provide adequate traction and load capacity. Thus, the wheels with vulcanised rubber coverings can have diverse mechanical characteristics. The most important parameters that define the quality of vulcanized rubber wheels are: hardness, density, impact strength, tensile strength and wear rate. During the injection molding process, the material is injected into the mold through a process of chemical synthesis, whereby the rubber retains its properties after molding.

The polyurethane wheel covering actually represents an elastomer that was created on the basis of the synthesis of the appropriate raw materials. Polyurethanes are chemical compounds obtained by mixing two components in liquid state triggering the polymerization reaction. The resulting mixture is cast into appropriate moulds or directly injected into heated moulds that have plastic or metal bases. In this way, different elastomers with the desired mechanical characteristics are formed. For example, mould-on polyurethane has good elasticity characteristics, while injected polyurethane has inferior elasticity characteristics, but superior hardness compared to mould-on polyurethane.

The centre and the covering of the monolithic (hard tread) wheel are made of the same material. The most frequently used materials for this type of the wheels are cast iron and thermoplastic materials. These materials determine the physical and mechanical characteristics of the wheel.

The pneumatic wheel covering is made of a rubber tyre with ply insert and an inner tube. The tread is usually grooved to increase the wheel-ground grip potential.

The wheels of material handling devices were analysed for different experimental load conditions using numerical analysis in [3]. The maintenance strategy of driving wheels and the influencing parameters on the wear process were analysed in [4].

1. THE BASIC ELEMENTS OF THE INDUSTRIAL WHEELS

The industrial wheel has the following components: the tread, the covering, the core, the hub and the swivel bearing, Figure 1 [5].
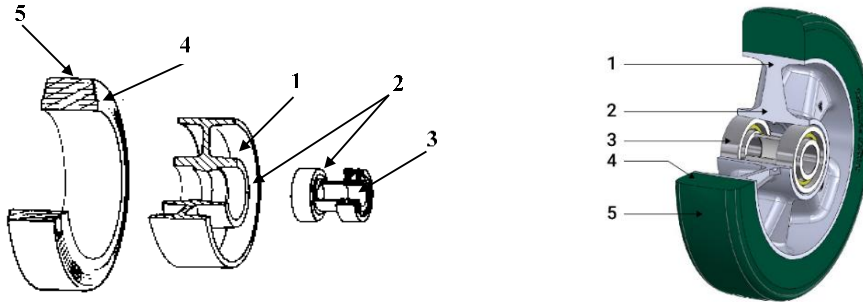
Figure 1. Basic industrial wheel components: core (1), hub (2), swivel bearing (3), covering (4), tread (5) [5]

The wheel tread is probably the most important part of the wheel, because it comes into direct contact with the ground. The tread can be smooth or with patterns that improve the wheel performance in critical areas such as noise, handling, grip and tire wear.

The wheel covering represents an outer ring and it is made of different materials. It is fixed to the wheel core using an adhesive or a mechanical connection.

The wheel core is the wheel element on which the wheel covering is mounted. It is built as a single element or as several elements joined together that connect the wheel covering with the wheel hub. The wheel core shapes can be made of a large number of different materials.

The wheel hub is the central, cylindrical part of the wheel. The wheel axle and the bearing are directly connected to it, so the hub participates in facilitation of the wheel rotation.

Most types of industrial wheels need the bracket to be connected to the equipment. There are two types of wheel brackets: the fixed type and the swivel type. The fixed brackets do not permit the change in direction of the equipment and they must be placed parallel to each other. The swivel bracket rotates about its own vertical axis which is offset with respect to the wheel vertical axis, providing good manoeuvrability of the equipment. There are several forms of the brackets, depending on the type of attachment with the equipment, Figure 2.

| a) | b) | c) | d) |
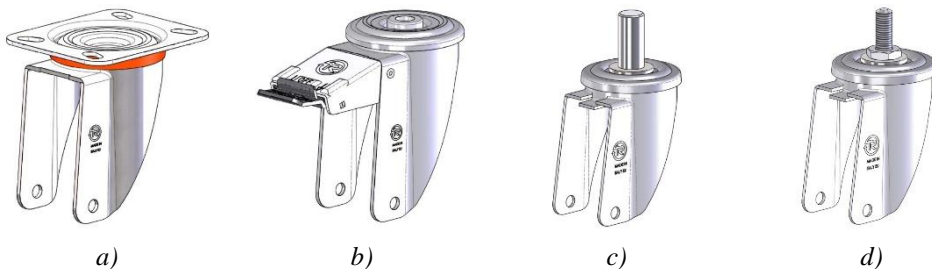
Figure 2. The swivel brackets for industrial wheels: a) plate swivel bracket, b) bolt hole swivel bracket, c) smooth stem swivel bracket, d) threaded stem swivel bracket [5]

2. SELECTING THE RIGHT WHEEL

In order to select the most economical solution for the wheels applied on the given internal transport device, it is necessary to define the working conditions and all external influencing factors. The right wheel can be selected as the result of the analysis of the following factors:

- type and condition of the ground surface,
- working environment,
- load parameters,
- equipment speed and traction devices and
- demands on equipment manoeuvrability.

There are three phases in selection of the right wheel according to the working conditions:

- identification of the correct type of the wheel based on the floor type and working environment,

- determination of the wheel diameter by calculating the static load, the dynamic capacity and smoothness required by the specific application,

- identification of the correct bracket and verification of the dynamic capacity of the wheel and bracket set.

The type and condition of the floor and the existing obstacles must be considered while selecting the wheel appropriate for given application. These factors also influence the performance of the moving equipment and the efficiency and the life span of the wheels and brackets. In the case the wheels are moving over uneven floors or over some obstacles, the magnitude of the generated resistance forces depends on the elasticity of the wheel covering material. The wheel with the elastic covering absorbs the greater amount of energy than the wheel with the rigid covering. Given the same load capacity, the greater diameter should be chosen for the wheels surpassing the obstacles than for the wheels going over uneven floors.

For each type of the industrial wheel, the standard working conditions are prescribed. Thus, in order to select the right wheel, it is imperative to determine whether the materials used to make the wheel covering, the wheel core, the wheel bearing and the bracket meet the specific requirements of working conditions (chemical conditions, temperature, humidity, inductive phenomena). Special attention must be given to operating conditions with aggressive agents. If there are oils, fats and hydrocarbons in the operating environment of the wheels, a polyurethane wheels should be selected, while in humid environments, the stainless steel brackets should be used.

Load parameters have a great effect on wheel load capacity. The general formula for calculation of the wheel load capacity is:

$$Q = \frac{P_u + P_c}{n} \qquad (1)$$

where: Q is the load capacity of each wheel, P_u is the weight that should be transported, P_c is the trolley weight and n is the number of wheels in contact with the floor.

Since the industrial wheels are exposed to fatigue due to a high number of stress cycles, the wheel with appropriate dynamic load capacity can be chosen from manufacturer's catalogues.

The speed of the equipment must be taken as the factor in selecting the right wheel. If the equipment is used mainly in static conditions (speed equals zero), then the load capacity of each wheel should be compared with catalogue values of the wheel manufacturers. If the speed has non-zero values, than the used traction devices should be considered (manual or mechanical). Manual traction implies that the traction force comes from one or more persons, while mechanical traction means that there is a mechanical device (on-board drive or towing device) which exerts the traction force.

Manoeuvrability is the ability of the equipment to easily move around the limited spaces and on the difficult routes. Good manoeuvrability features of the equipment make the operator tasks easier.

The most common wheel layouts are shown in Table 1 [5].

Table 1. The most common wheel layouts [5]

DIAGRAM	CASTOR LAYOUT	OPERATING CONDITIONS	APPLICATION EXAMPLES
	Stable trolley: two wheels with swivel castor and two wheels with fixed castor	Long and straight routes Few direction changes	Mechanical workshops, semi-automated warehouses, metallurgical workshops.
	Stable trolley: four wheels with swivel castor	Short routes Frequent direction changes Approach to machines or shelves	Supermarkets, wood machining companies, small distribution centres.
	Stable trolley: one wheel with swivel castor and two wheels with fixed castor	Long and straight routes Few direction changes	Small trolleys Tool/object carriers Light loads
	Tipping trolley: two wheels with fixed castor and four wheels with swivel castor	Long routes with mechanical towing Few direction changes	Moving in railway, postal, airport areas. Heavy loads
	Tipping trolley: four wheels with fixed castor	Long and straight routes without direction changes	Assembly or machining lines with round trip and head transfer device
	Tipping trolley: two wheels with fixed castor and two wheels with swivel castor	Long routes with manual or mechanical towing Few direction changes	Mechanical and metallurgical workshops, semi-automated warehouses
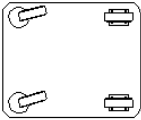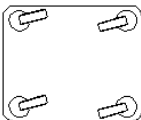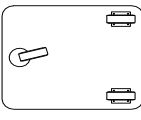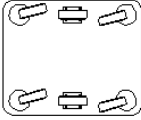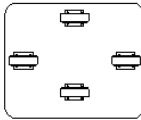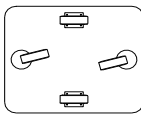
Based on required load capacity and working speed and on the adopted wheel materials, the working diameter of the wheel is defined.

Potential choice of the wheel materials is listed in Figure 3.
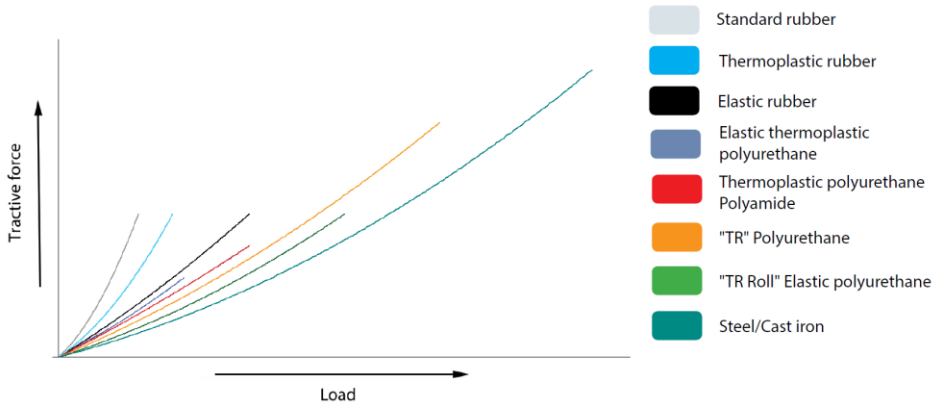
Figure 3. Comparison chart of the rolling resistance between the different wheel materials

3. THE USE OF INDUSTRIAL WHEELS AND BRACKETS IN LOGISTICS AND IN HANDLING OPERATIONS

A vast variety of material handling devices are used during production and transport processes in automotive industry. During the process of lifting and transporting the materials, different types of industrial wheels and brackets are used, as shown in Figures 4 to 6. Figure 6 also indicates the use of full automation using roller or chain conveyor.

Figure 4. Polyurethane wheels with aluminium core

Figure 5. Polyurethane wheels with cast iron core

Figure 6. Polyurethane wheels with aluminium core

Equipment for car repair shops is shown in Figure 7, while characteristic types of corresponding industrial wheels are given in Figures 8 and 9.

Figure 7. Equipment for car repair shops

Figure 8. Polyurethane wheels with aluminium core

Figure 9. Solid polyamide wheels

An integral part of automotive warehouses is a variety of equipment for moving pallets, ranging from manual devices to computer-controlled devices. The most often used devices are: wheeled forklifts, hand pallet trucks, motorized pallet trucks, conveyors and automated guided vehicles (AVGs).

The forklift trucks are devices that are used very often due to their ability to actively pick up and dispose the pallets, but also to stack the load by height, Figure 10. Their mobility is limited by the aisle widths in which they are used. Optimal aisle width should allow the forklift truck to be positioned at the right angle to the aisle. Wider aisles offer more flexibility in picking pallets and immediate loading to the trailers, which implies greater travel speeds and lower cost of operation of wide aisle trucks. However, using narrow aisles

brings greater overall storage density [6]. This means that there should be balance between wheeled truck speed of operation, proper choice of their wheels, storage density and costs.

The wheels of forklift trucks often have polyurethane tyres. These tyres act better on slippery floors and can lift up to 15% heavier loads than rubber tyres. They offer smoother ride and do not leave permanent marks on the floor. The wheels of electric pallet trucks also have polyurethane tyres that enable high speed handling [7].

Some of the wheels and rollers for pallet trucks, stackers and other forklift trucks are shown in Figure 11 to Figure 13.

Figure 10. Forklift trucks

Figure 11. Polyurethane transpallet rollers with steel core

Figure 12. Polyurethane drive wheel

Figure 13. Customised solutions

The heavy duty industrial wheels are made of different materials [5]:

- polyurethane (great resistance to wear and deformations),
- elastic polyurethane (polyurethane with the ability to overcome obstacles, avoid noise, suppress vibrations),
- "Vulkollan" elastomer,
- PA6 (polyamide 6), or
- cast iron.

The wheels made of the above mentioned materials can be also used on the trolleys for the automotive industry.

The wheels of electric pallet trucks, Figures 14 and 15, also have polyurethane tyres that enable high speed handling [8]. Other used types of the wheels include: solid polyamide wheels, Figures 16 to 18, and elastic rubber wheels with aluminium core, Figure 19.

Figure 14. Hand pallet truck

Figure 15. Power pallet truck

Figure 16. Solid polyamide wheels

Figure 17. Complete solid polyamide wheels

Figure 18. Polyamide transpallet rollers

Figure 19. Elastic rubber wheels with aluminium core

Mechanical tugger train compositions are often used in automotive industry. They consist of a train truck and a number of train elements, trailers and trolleys, Figure 20. The train capacity depends on the number of coupled elements [1]. The trolleys have four swivel wheels, Figure 21. Different types of trolleys can contain different designs and dimensions of wheels, Figures 22 and 23.

The trolley and roll container systems (Figures 24 to 26) facilitate the transport of goods and are applicable in many industries and at airports, railway stations and bus stands. They are suitable for medium loads, for indoor-outdoor use and they do not leave marks on the floor.

Figure 20. Tugger trains composition
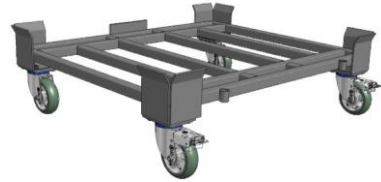
Figure 21. Trolley of mechanical tugger train

Figure 22. Injection polyurethane transpallet rollers with polyamide centre

Figure 23. Polyurethane wheels with aluminium centre

Special trolleys can contain extra heavy duty welded brackets. Characteristic wheel solutions for these systems are shown in Figures 27-32.

Figure 24. Platform trolley

Figure 25. Tool trolley

Figure 26. Roll container

Figure 27. Standard rubber wheel with pressed steel disc

Figure 28. Thermoplastic rubber wheel with polypropylene centre

Figure 29. Solid polyamide wheel

Figure 30. Polyurethane wheel with aluminium centre

Figure 31. Sigma elastic rubber wheel with polyamide centre

Figure 32. Solid red polyamide wheel

Storage and retrieval machines are a special type of cranes for working in warehouses. The main difference compared to forklift trucks is that they are not freely rotating machines, but are attached to rails on the floor or on the ceiling. They move in a straight line through the corridors between the racks, Figure 33. The wheel of these machines are mostly heavy duty industrial polyurethane wheels with cast iron core, Figure 34. Sometimes they use customized solutions for driving wheels in order to meet the required carrying capacity of the transport system, Figure 35.
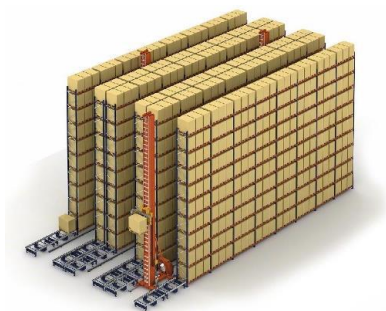
Figure 33. Storage and retrieval machines

Figure 34. High performance polyurethane drive wheels

Figure 35. Customized solutions

In order to fulfil the investor's basic request to obtain the largest possible storage capacity in the available space, i.e. to store the largest possible amount of material, storage designers must know all the possibilities of transport and handling equipment [8]. In this sense, attention must be paid to:

- type and form of the chosen transport device,
- method of control (manual or electric),
- inertial forces due to acceleration and braking (if the steering is electric),
- additional dynamic effects due to braking, accelerating or turning (if a person controls the vehicle),
- wheel diameters,
- wheel material (steel, rubber, polyurethane) and
- distribution of the load on the wheels.

4. CONCLUSIONS

Different internal transport and handling devices in automotive industry utilize a number of different types of industrial wheels. In general, the optimal choice of the wheels for internal transport devices should be based on the following criteria:

- effective use of space,
- low levels of floor damage,
- high speed of throughput,
- minimum overall system cost and
- personnel safety.

The selection of the appropriate type of wheels also depends on: type and condition of the floor, existence of obstacles, operating conditions, load parameters and equipment operating speed.

The wheels for material handling equipment should be made of high-quality materials that provide low-noise operation, very low rolling resistance, high dynamic load capacity, good floor preservation and high abrasion resistance.

REFERENCES

[1] Vujanac R., Djordjevic M., Miloradovic N.: "Mechanical tugger trains system for internal material handling", The proceedings of the 6th international conference "TRANSPORT AND LOGISTICS" (TIL 2017), pp. 73-76, 25th - 26th May 2017, Nis, Serbia, 2017, ISBN 978-86-6055-088-2.

[2] Rushton A., Croucher P., Baker P.: "The handbook of logistics and distribution management", 4th edition, Kogan Page Limited, London, 2010.

[3] Cima M., Solazzi L.: "Experimental and analytical study of random fatigue, in time and frequencies domain, on an industrial wheel", *Engineering Failure Analysis*, Vol. 120, No. 105029, 2021, DOI:10.1016/j.engfailanal.2020.105029

[4] Chang M., Lee J.: "Early stage data-based probabilistic wear life prediction and maintenance interval optimization of driving wheels", *Reliability Engineering and System Safety*, Vol. 197, No. 106791, 2020. DOI:doi.org/10.1016/j.ress.2020.106791

[5] Tellure Rôta S.p.A.: Catalogue, Formigine, Italy, 2023.

[6] Miloradović N., Vujanac R., Stojanović B.: "Stacking aisle width for forklift trucks in palletized storage and handling systems", the 10th Anniversary International Conference on Accomplishments in Electrical and Mechanical Engineering and Information Technology DEMI 2011, Banja Luka, 26th – 28th May 2011, pp. 899-904, 2011, ISBN 978-99938-39-36-1.

[7] Brito A., How polyurethane can be used in today's manufacturing industry, *Reinforced Plastics*, Vol. 64, Number 5, September/October 2020

[8] Vujanac R., Miloradovic N.: "Basics of storage and transport systems" (in Serbian), Faculty of Engineering, University of Kragujevac, Kragujevac, 2023.

Intentionally blank

EXPERIMENTAL DEFINING OF NORMAL ANISOTROPY COEFFICIENT AS FORMABILITY FACTOR OF THIN CAR BODY SHEETS

Srbislav Aleksandrović [1]*, Darko Perić [2]

ABSTRACT: It is well known that anisotropy have very significant influence on car body sheet metals formability in deep drawing process. At the other hand deep drawing is essential technology of all car body parts. Anisotropy can be observe as planar and orthogonal (normal). For deep drawing more significant is normal anisotropy which is represent by coefficient of normal anisotropy or plastic strain value or so called "r" factor. It is numeric value which is obtaining experimentally by uniaxial tension in field of homogenous plastic strain. There is no precise recommendation about intensity of maximal allowed plastic strain during the tensile experiment. In this paper presented is experimental investigation of smaller plastic strains intensities influence on final "r" value. Used are two thin sheet metals: stainless steel X5CrNi18-10, 0.8 mm nominal thick and Al alloy sheet AlMg4.5Mn0.7 (i.e. ENAW 5083) 1 mm nominal thick where the samples are cut in the rolling direction for both materials. Plastic strain was relate to maximal homogenous plastic strain A_g in the following way: 10, 20, 30, 40, 50, 60, 65, 70 and 75 percent of A_g. After the results evaluation can be concluded that there is relatively small influence of plastic strain intensity on "r" value occurred i.e. determining of "r" value can be successfully obtained with smaller intensity of plastic strain.

KEY WORDS: *car body sheet metals, anisotropy, "r" value*

[1] *Srbislav Aleksandrovic, Faculty of Engineering, University of Kragujevac, Sestre Janjic 6, Kragujevac, Serbia, srba @kg.ac.rs, ⓘ 0000-0001-5068-5560 (*Corresponding author)*
[2] *Darko Peric, master student, Faculty of Engineering, University of Kragujevac, Sestre Janjic 6, Kragujevac, Serbia, darkoperic2322@gmail.com, ⓘ-*

EKSPERIMENTALNO ODREĐIVANJE KOEFICIJENTA NORMALNE ANISOTROPIJE KAO FAKTORA DEFORMABILNOSTI KAROSERIJSKIH LIMOVA

Srbislav Aleksandrović, Darko Perić

REZIME: Dobro je poznato da anizotropija ima veliki uticaj na deformabilnost karoserijskih limova u procesu dubokog izvlačenja. S druge strane, duboko izvlačenje je ključna tehnologija za sve delove karoserije vozila. Anizotropija može da se posmatra kao ravanska i normalna. Za duboko izvlačenje znatno je važnija normalna, koja se izražava preko koeficijenta normalne anizotropije ili tzv. "r" faktora. To je brojna vrednost koja se određuje eksperimentalno jednoosnim zatezanjem u oblasti ravnomerne plastične deformacije. Ne postoje precizne preporuke u vezi intenziteta najveće dozvoljene plastične deformacije tokom procesa. U ovom radu je dato eksperimentalno istraživanje uticaja manjih vrednosti plastičnih deformacija na konačnu vrednost "r" faktora. Korišćena su dva lima: čelik X5CrNi18-**10,** nominalne debljine 0,8 mm i lim od Al legure AlMg4,5Mn0,7 nominalne debljine 1 mm, pri čemu su epruvete sečene u pravcu valjanja za oba materijala. Plastična deformacija je bila vezana za maksimalnu ravnomernu plastičnu deformaciju A_g na sledeći način: 10, 20 30, 40, 50, 60, 65, 70 i 75 procenata od A_g. Posle razmatranja rezultata može se zaključiti da postoji relativno mali uticaj intenziteta plastične deformacije na vrednost "r" faktora, t.j. da se vrednost "r" faktora može uspešno odrediti i pri manjim stepenima deformacije.

Ključne reči: karoserijski limovi, anizotropija, "r" faktor

EXPERIMENTAL DEFINING OF NORMAL ANISOTROPY COEFFICIENT AS FORMABILITY FACTOR OF THIN CAR BODY SHEETS

Srbislav Aleksandrović, Darko Perić

INTRODUCTION

Car body structure (Fig. 1), including outer panels, is being made almost from steel and Al alloys sheets. Main technology in forming processes is deep drawing. In these processes very important is to know how to evaluate formability of sheet materials. In numerous researches [1, 2, 3, 4, 5 etc] has been established that relatively simple but effective way to evaluate sheet metals formability in deep drawing processes is determination of anisotropy parameters, especially normal (orthogonal) anisotropy parameters.

Figure 1. Car body structure

Car body thin sheet metals are almost always anisotropic materials. Anisotropy can be expressed as plane i.e. planar and normal (orthogonal). Plane anisotropy is related to different mechanical and formability characteristics variation considering different directions in sheet metal plane, where the referent direction is the rolling direction. Normal anisotropy is related to the direction of 90 degree towards the sheet surface i.e. in the direction of sheet thickness, and that material property has a special importance. It was theoretically considered for a long time that is most suitable for the sheets to be isotropic. It is the state where the properties are equal in all directions in volume. In technological practice, the opposite conclusion was reached very soon. Actually, very convenient is the situation where deformations in sheet plane are large but at the same time thickness deformation (thinning or thickening) very small.

The significance of the influence of the "r" factor on deep drawing formability can be seen in Fig. 2. There is a high degree of correlation between "r" factor and LDR of cylindrical sheet metal part. As the value of the "r" factor increases above 1, the LDR also increases intensively.

The most suitable parameter to express normal anisotropy is parameter known by several names: coefficient of normal anisotropy, plastic strain ratio, "r" value, "r" factor etc. Here in the text the term "r" factor is adopted. In addition to its importance as a formability parameter "r" factor is important parameter in anisotropic plasticity theory and numerical

simulation of metal forming processes. "r" factor can be determined experimentally only ([4], [5], [6], [7], [8]) and it's a matter of standards ([9], [10]). "r" factor is important parameter for consideration of anisotropy influence in different forming processes beside deep drawing, or theory investigations (e. g. [11]). Many studies have been devoted to the influence of anisotropy for specific materials and technological processes (e.g. [12], [13]).
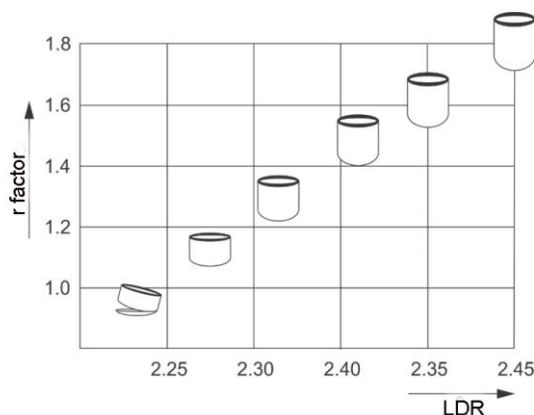
Figure 2. Limiting drawing ratio (LDR) dependence on "r" factor

Main experimental procedure for "r" factor determination is uniaxial tension in a field of a homogenous plastic strain. In standards ([9], [10]), scientific articles ([5], [8] etc). and other publications ([1] etc). there is no exact recommendation about intensity of that strain which must be given. Recommendation are general and because of that there is a space for research and answer the question: how given intensity of plastic strain affects the final value of "r" factor for different materials. Here in this paper special attention is paid to the influence of low intensities of plastic strains. In article [14] given is extensive investigation of the influence of strain higher degrees and sample geometries both. This article actually gives continuations of those researches.

1. EXPERIMENT

Procedure for "r" factor experimental determination is uniaxial tension, as previously noted. In [14] concluded was that there is no important influence of sample geometry on the "r" factor final value. So, here is adopted specimen geometry given at Fig. 3.
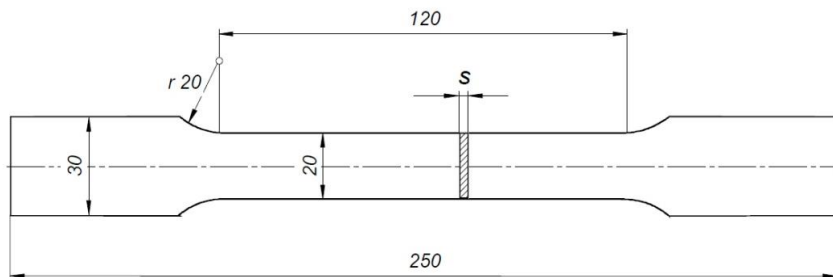
Figure 3. Specimen geometry for uniaxial tension

The definition of the "r" factor is given by well-known formulas:

$$r = \frac{\varphi_b}{\varphi_s} = \frac{ln\frac{b_0}{b}}{ln\frac{s_0}{s}} \qquad (1)$$

$$l_0 \cdot b_0 \cdot s_0 = l \cdot b \cdot s = const. \qquad \frac{s_0}{s} = \frac{l \cdot b}{l_0 \cdot b_0} \qquad r = \frac{ln\frac{b_0}{b}}{ln\frac{l \cdot b}{l_0 \cdot b_0}} \qquad (2)$$

where φ_b is logarithmic (true) plastic strain of specimen width; φ_s is logarithmic (true) plastic strain of specimen thickness, l_0, b_0, s_0 are initial specimen dimensions, length, width and thickness; l, b, s are in process, or final, specimen dimensions, length, width and thickness. It is useful to note that for much higher accuracy, width measurement is used instead of thickness measurement. Measuring of the width changes usually performs at several places (up to nine) and then calculate average value ([8], [9], [10], [14]).

If the "r" factor r=1 there is isotropic sheet, i.e. deformation in sheet plane is equal as the deformation of thickness. If r<1 thickness deformation (thinning) is higher than deformation in sheet plane. This situation is inconvenient because thinning quickly leads to localized deformation and fracture appearance. Suitable situation is r>1. The higher r is than 1, the larger is the deformation in the plane of the sheet and the lower is thinning. In practice, the most suitable values of the "r" factor are r>1.2 [1]. "r" factor actually represent resistance of the material to thinning which can be dangerous because of fracture appearance.

Materials used in the experiment are: austenitic stainless steel sheet X5CrNi18-10 with measured mechanical properties (Fig. 4): tensile strength R_M=679,2 MPa, flow stress R_P=266,5 MPa, percentage elongation at fracture A=62,1% and percentage elongation at maximal force i.e. maximal homogenous strain Ag≈60%; Al alloy AlMg4,5Mn0,7 (or ENAW 5083) sheet metal with properties (Fig. 5): tensile strength R_M=253,5 MPa, flow stress R_P=109,2 MPa, percentage elongation at fracture A=24,4% and percentage elongation at maximal force i.e. maximal homogenous strain Ag=23%; Al alloy temper is F (fabricated, as cast) [15]. Samples was cut in rolling direction. Should be noted that this Al alloy sheet metal is intended for cold forming and can be successfully used for car body parts.
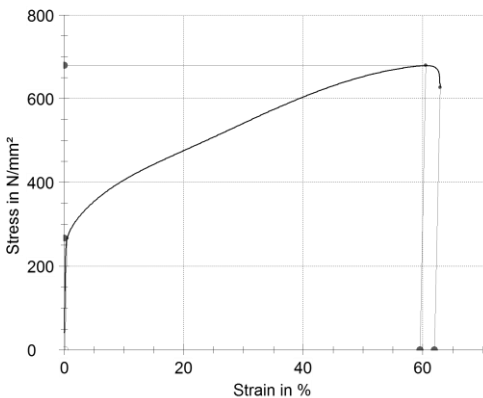
Figure 4. Stress-strain curve for stainless steel
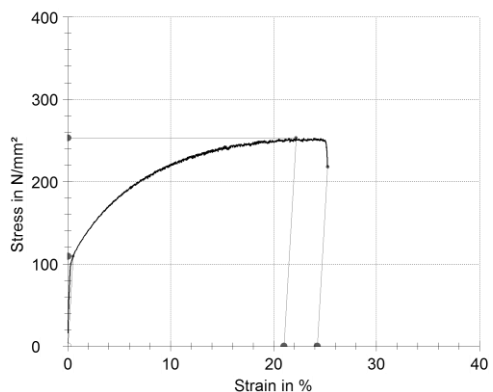
Figure 5. Stress-strain curve for Al alloy

For investigate the influence of the intensity of plastic strain first were determined reference values i.e. percentage elongations at maximal force for both materials. That is the preparatory part of the experiment. In relation to those values, a series of strain values that should be set is defined. The following plastic strain values are selected: 10, 20, 30, 40, 50, 60, 65, 70, 75 percent of Ag.

The experiment was performed on computerized tensile machine Zwick/Roell Z 100 (Fig. 6). The physical appearance of one series of specimens is given in Fig. 7.
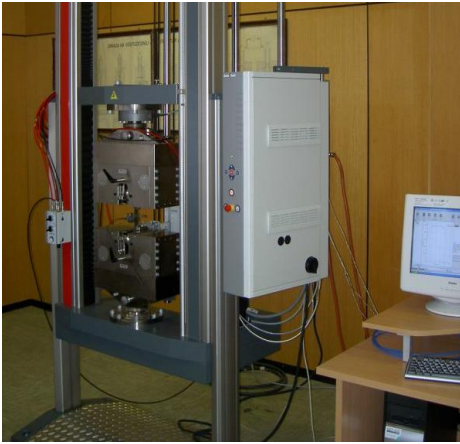
Figure 6. Computerized tensile machine   *Figure 7. One series of specimens*
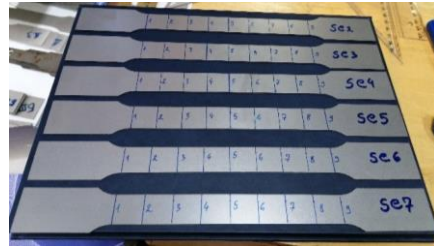
It should be noted here that it is necessary to reject all the general and imprecise recommendation and perform uniaxial tensile testing with a aim of determining the real values of maximal homogenous strains. Later can be adopted appropriate value of plastic strain necessary for "r" factor.

2. RESULTS AND CRITICAL CONSIDERATIONS

After defining the required intensities of plastic strains, it was started with uniaxial tension tests. There were difficulties with elastic strains that needed to be determined as exactly as possible. This was done in previous experiments. Influence of the elastic strains must be eliminated. In Table 1 and Table 2 given are the results. Values for **b** (appropriate width change) and **l** (appropriate length change) are related to the pure plastic strain without elastic strain. Realized plastic strains values are signed as percent of maximal homogenous strain Ag, and can be calculated from l_0, and **l**.

Table 1. Results for X5CrNi18-10 sheet metal

b_0 [mm]	b [mm]	l_0 [mm]	l [mm]	s_0 [mm]	% of Ag	r [-]
20,08	17,41	118,4	166,0	0,77	75	0,731
20,06	17,61	116,6	157,8	0,76	70	0,755
20,06	17,76	117,9	156,4	0,76	65	0,757
20,06	17,89	117,5	153,4	0,77	60	0,752
20,10	18,23	117,4	147,8	0,76	50	0,736
20,06	18,50	116,8	140,6	0,76	40	0,744
20,04	18,85	118,2	136,2	0,76	30	0,760
20,06	19,21	118,0	130,6	0,76	20	0,744
20,08	19,64	118,3	125,0	0,77	10	0,673

Table 2. Results for AlMg4.5Mn0.7 sheet metal

b_0 [mm]	b [mm]	l_0 [mm]	l [mm]	s_0 [mm]	% of Ag	r [-]
19,93	19,04	116,2	135,8	1,06	75	0,472
19,93	19,05	118,0	135,6	1,06	70	0,481
19,93	19,07	117,8	134,2	1,06	65	0,511
19,91	19,12	117,8	132,6	1,07	60	0,520
19,93	19,22	117,0	130,0	1,06	50	0,525
19,94	19,42	116,6	126,8	1,06	40	0,460
19,90	19,48	117,3	125,2	1,06	30	0,486
19,94	19,68	117,4	123,2	1,07	20	0,374
19,93	19,79	117,4	120,6	1,06	10	0,354

Figure 8 and Figure 9 shows tensile diagrams for part of the experiment. Figure 8 are related to steel sheet, and Figure 9 to Al alloy sheet. It should be noted that the curves in the diagrams show the realized previously given plastic strains. The curves are shown with the appropriate offset, i.e. the distance between them.
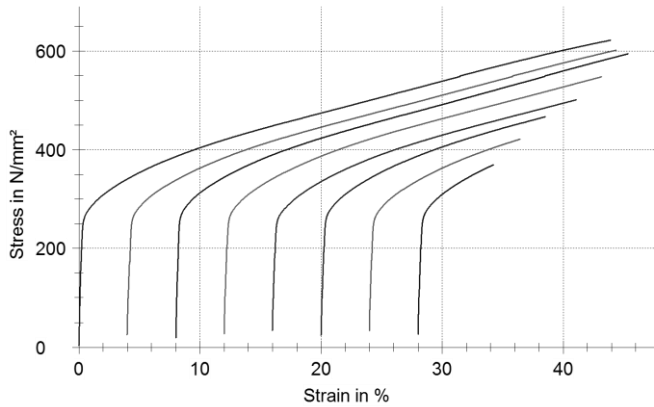
Figure 8. Tensile diagrams for X5CrNi18-10 sheet
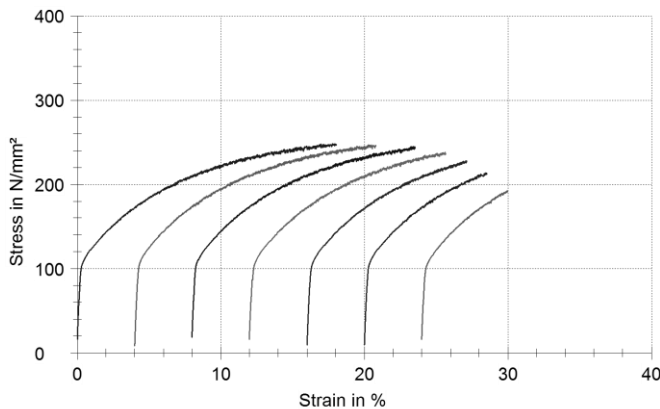
Figure 9. Tensile diagrams for AlMg4.5Mn0.7
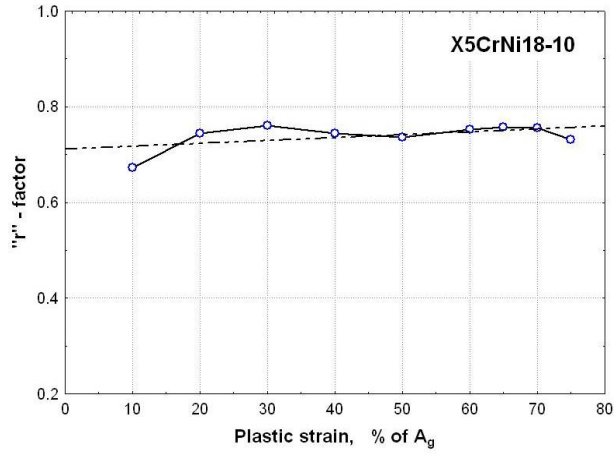
Figure 10. "r" factor dependence on plastic strain
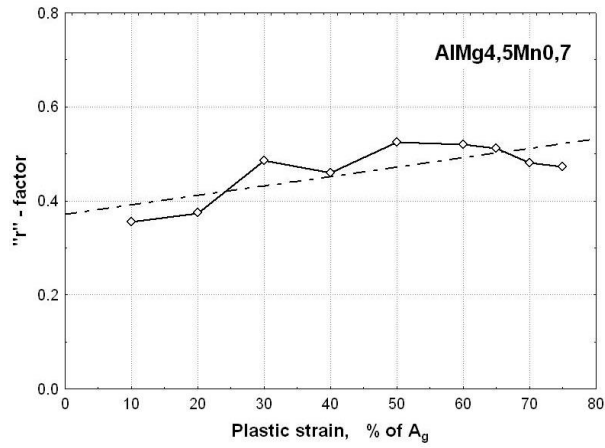
Figure 11. "r" factor dependence on plastic strain
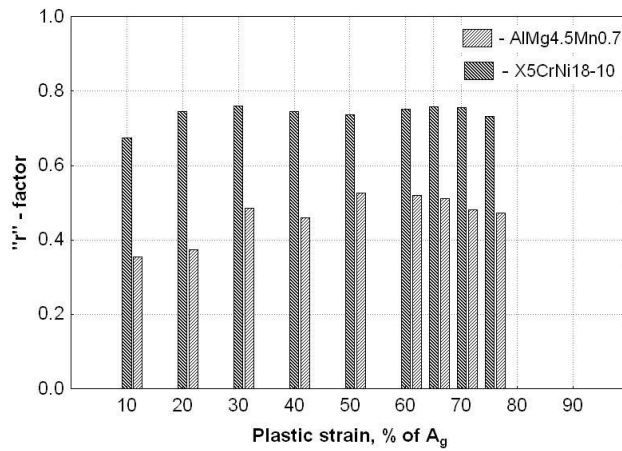
Figure 12. "r" factor dependence on plastic strain

Based on the results in Table 1 and Table 2 the diagrams in the Figure 10 and Figure 11 were formed, and also histogram in Figure 12. Diagrams and histogram shows "r" factor dependence on previously set plastic strain signed as percent of maximal homogenous strain Ag. Clearly can be seen the influence of the degree of deformation on "r" factor value. The formed curve for steel sheet deviates relatively little from the slightly inclined straight line representing the average value. Irresistibly conclusion is that a large decreasing of plastic deformation has a relatively small, almost negligible effect on the values of the "r" factor.

For the Al alloy sheet the situation is somewhat different. First, inclination of the straight average line is larger than the steel. Second, points deviations from average line are larger. Therefore, the conclusion is not so clear, although as the plastic strain decreases, the "r" factor value also decreases to a certain extent. The histogram from Figure 12 shows the same as Figure 10 and Figure 11.

The probable reasons for the previous considerations are, firstly, the materials are completely different, and secondly, the realized absolute intensities of plastic strains are also very different. Plastic strain absolute intensity of Ag for sheet X5CrNi18-10 is 60%. Ten percent of that is 6%. Plastic strain absolute intensity of Ag for sheet AlMg4.6Mn0.7 is 23%. Ten percent of that is 2.3%, almost 3 times lower. Therefore, one can be careful and use plastic strain closer to Ag for determining the "r" factor in materials with lower plasticity. Something is different in the case of material with better plasticity like with austenitic stainless steel in this case. There is possible to use significantly less intensities of the plastic strains without reducing measuring accuracy.

3. CONCLUSIONS

After considering the results of the conducted experiment, the following observations and conclusions can be made:

- the influence of the type of material on the "r" factor value determination related to the application of different intensities of plastic strains is clearly visible,
- with materials that have better plasticity lower intensity of plastic strain can be used,
- with materials that have lower plasticity must be used intensity of plastic strain closer to Ag,
- in the experiment, one should be careful of the harmful influence of elastic deformations, which must be eliminated,
- in the following investigations, the intensities of plastic strains and their range should be defined even more carefully,
-also, in the following investigations it would be useful to include more different materials.

AKNOWLEDGEMENT

REFERENCES

[1] Devedžić, B.: Plastičnost i obrada metala deformisanjem (Plasticity and metal forming), Naučna knjiga, Beograd, (p. 64-65, 250-254), 1992. (In Serbian)

[2] Aleksandrović, S., Stefanović, M.: Tehnologija plastičnog oblikovanja metala (Technology of metal plastic forming), Mašinski fakultet Univerziteta u Kragujevcu, 2010. (In Serbian)

[3] Aleksandrović S.: Sila držanja i upravljanje procesom dubokog izvlačenja (Blank holding force and deep drawing process control), Mašinski fakultet Univerziteta u Kragujevcu, (p. 18) 2010. (In Serbian)

[4] Aleksandrović, S.: Deformabilnost – Anizotropija (Deformability - Anisotropy), lecture for FIAT Automobili Srbija, Fakultet inženjerskih nauka Univerziteta u Kragujevcu, 2014. (In Serbian)

[5] Danckert, J., Nielsen, K.B.: Determination of the plastic anisotropy r in sheet metal using automatic tensile test equipment, Journal of Mat. Proc. Technology, ISSN 0924-0136, vol. 73, p. 276-208., 1998, https://doi.org/10.1016/s0924-0136(97)00238-0.

[6] Aleksandrović, S., Stefanović, M., Adamović, D., Lazić, V.: Variation of Normal Anisotropy Ratio „*r*" During the Plastic Forming, Journal of Mechanical Engineering, ISSN 0039-2480, vol. 55, p. 392-399, 2009.

[7] Aleksandrović, S.: Savremeni postupci plastičnog oblikovanja (Advanced procesess of plastic forming), script, Fakultet inženjerskih nauka Univerziteta u Kragujevcu, 2018. (In Serbian)

[8] Gedney, R.: Measuring the Plastic strain Ratio of Sheet Metals, ADAMET Inc., Norwood, MA, USA, 2005.

[9] Standard ISO 10113:2020(E): Metallic materials — Sheet and strip— Determination of plastic strain ratio, International Organization for Standardization, Geneva, Switzerland, p. 1-7, 2020.

[10] ASTM Standard E 517-00: Standard test method for Plastic Strain Ratio r for Sheet Metal, Annual Book of ASTM Standards, ASTM, West Conshohocken, PA, USA, 2002.

[11] Banabic, D.: Advances in Plastic Anisotropy and Forming Limits in Sheet Metal Forming, Journal of Manufacturing Science and Engineering, ISSN 1087-1357, vol. 138, p. (090801-1)-090801-9)., 2016, https://doi.org/ 10.1115/1.4033879.

[12] Ailinei, I.I, Galatanu, S,V., Marsavina, L.: Influence of anisotropy on the cold bending of S600MC sheet metal, Engineering Failure Analysis, ISSN 1350-6307, vol. 137, no. 106206, 2022, https://doi.org/10.1016/j.engfailanal.2022.106206

[13] Tardif, N., Kyriakides, S.: Determination of anisotropy and material hardening for aluminum sheet metal, International Journal of Solids and Structures, ISSN 0020-7683, vol. 49, p. 3496-3506., 2012, https://doi.org/10.1016/ j.ijsolstr.2012.01.011.

[14] Srbislav Aleksandrović, Đorđe Ivković, Dušan Arsić, Marko Delić, Slaviša Đačić, Milan Đorđević: Effect of plastic strain and specimen geometry on plastic strain ratio values for various materials, Advanced technologies and materials, ISSN: 2620-0325 (print), ISSN: 2620-147X (online), Vol. 48, No.1, 2023, pp. 13 - 19, https://doi.org/10.24867/ATM-2023-1-003**.**

[15] Steel number, from: https://www.steelnumber. com (accessed on: March 22, 2024.)

CONTRIBUTION TO THE DEVELOPMENT OF A METHOD FOR OPTIMAL DIMENSIONING OF THE FRAME IN THE INITIAL DESIGN PHASE OF A HEAVY MOTOR VEHICLE

Miroslav Demić [1]*

ABSTRACT: As it is known, the parameters of a heavy motor vehicle, including the frame, are not known in the initial design phase of the vehicle. Therefore, in this paper, an attempt is made to define the necessary dimensions based on the minimization of its lateral vibrations, while simultaneously minimizing the mass and maximizing the moment of inertia of the cross-section of the frame.

Attention is given to the choice of the objective function in the optimization process, with a special focus on the interrelation of sub-objectives. The author's previously developed frame model and „stochastic parametric optimization" based on the Hooke-Jeeves method were used for the research.

The calculated value of the unknown frame parameter is intended to serve for the final selection of the frame structure in the later design phase.

KEY WORDS: *Heavy motor vehicle, frame, lateral vibrations, mass, moment of inertia, troparametric Fourier transformation*

[1]*Miroslav Demić, Faculty of Engineering, University of Kragujevac, Sestre Janjic 6, Kragujevac, Serbia, demic @kg.ac.rs, ⓘ: 0000-0001-5068-5560 (*Corresponding author)*

PRILOG RAZVOJU METODE ZA OPTIMALNO DIMENZIONISANJE OKVIRA U FAZI IZRADE IDEJNOG PROJEKTA TERETNOG MOTORNOG VOZILA

Miroslav Demić

REZIME: Kao što je poznato, parametri teretnog vozila, a samim tim i okvira, nisu poznati u početnoj fazi projektovanja, pa je, u ovom radu učinjen pokušaj definisanja potrebnh dimenzija, na bazi minimizcije njegovih poprečnjih vibracija, uz istovremenu minimizaciju mase i maksimizaciju momenta inercije poprečnog preseka okvira.

Pažnja je posvećena izboru funkcije cilja u procesu optimizacije, sa posebnim osvrtom na međusobni odnos podciljeva. Za istraživanje je korišćen ranije razvijeni autorov model okvira i "stohastička parametarska optimizacija" zasnovana na metodi Hooke-Jeeves-a.

Izračunata veličina nepoznatog parametra okvira treba da posluži za konačan izbor structure okvira u kasnijoj fazi projektovanja.

KLJUČNE REČI: *Teretno motorno vozilo, okvir, poprečne vibracije, masa, moment inercije, troparametarska Furijeova transformacija*

CONTRIBUTION TO THE DEVELOPMENT OF A METHOD FOR OPTIMAL DIMENSIONING OF THE FRAME IN THE INITIAL DESIGN PHASE OF A HEAVY MOTOR VEHICLE

Miroslav Demić

INTRODUCTION

The initial design phase of a heavy motor vehicle, defined by the design task, is further developed in subsequent design phases, where creative and intuitive settings that played a significant role in the development of the design task give way to logical and objective factors, calculations, measurements, shaping, evaluations of production and technological capabilities, etc. [1,2].

The assumption is that the design task defines that a heavy motor vehicle with a total mass of 11000, kg and a payload capacity of 4,000, kg needs to be designed for the market, with dimensions (length * width * height, mm): 6400*2500*3600, with a short cab. The engine is positioned at the front, and it has all-wheel drive.

The frame of the newly designed vehicle must withstand rigorous exploitation conditions, and it will be dimensioned using optimization methods based on minimal transverse vibrations and mass, and maximum moment of inertia of the transverse section.

The previously developed frame model and the "stochastic parametric optimization" based on the Hooke-Jeeves method will be used. Special attention will be given to the choice of the objective function and the analysis of the influence of sub-objectives on the optimizing parameter.

It is pointed out that optimization can be done:

•theoretically, using mathematical models and dynamic simulation,

•experimentally, and

•in a combined way.

It should be noted that experimental research is expensive and often not applicable in the initial phase of vehicle design. Therefore, the procedure of theoretical optimization is accepted here, which required modeling of the frame. It is noted that the author has previously developed a frame model, and it will be presented here with slight abbreviations that will not compromise the understanding of the method of the optimal selection process of its unknown parameter.

1. METHOD

As already mentioned, this paper aims to explore the possibility of applying optimal dimensioning of the frame in the initial design phase of a vehicle, using optimization methods. It was deemed appropriate that the objective function should enable the minimization of transverse frame vibrations and its mass, while maximizing the moment of inertia of the transverse section.

For further considerations, a ladder structure of the frame was adopted, as in [3], along with its length and width. Now, based on the required torsional stiffness of the frame, it is necessary to define the dimensions of the longitudinal and transverse profiles using some of the calculation methods, most commonly finite element methods [4]. It should be noted that

in this design phase, the bending and torsional stiffness, as well as precise external loads, are not known, so the application of the mentioned method is not possible with satisfactory reliability.

Considering that in this design phase, a large number of frame parameters are unknown and some of them must be obtained through the study of simpler models, it was deemed appropriate to idealize and observe the frame as a homogeneous plate of adopted length and width, with unknown thickness [3], Figure 1a). The plate undergoes transverse vibrations under the influence of disturbing forces at the connection points of aggregates, systems, and the frame...

For motor vehicles [2], there are statistical data on the percentage participation of aggregates and systems in the vehicle's own mass. Based on the design requirement, a frame length of 6100, mm and a width of 800, mm were adopted, so based on the data from [2], the thickness of the equivalent plate (idealized steel frame) was calculated to be 23, mm [3].

In order to analyze the transverse vibrations of the frame model, it was necessary to define dynamic excitations. Considering that not all excitations are known in this project phase (uneven engine operation, road irregularities, tire non-uniformity, etc.), it was deemed appropriate to analyze vibrations under conditions of short-term intensive braking [3,5]. Based on experience, an impulse decceleration shape was chosen with the presence of random changes, as illustrated in Figure 1b) [3].

For further analysis, it was adopted that the engine is supported by the frame at four mounts, the cab also at four points [1,3]. The cargo box is supported at eight mounts, but for the sake of problem simplification, it was assumed that it is attached to the frame at four points. As for the springs, each of them is connected at two points, but for the same reasons as with the cargo box, it was assumed that they are connected at one point each [1,3].
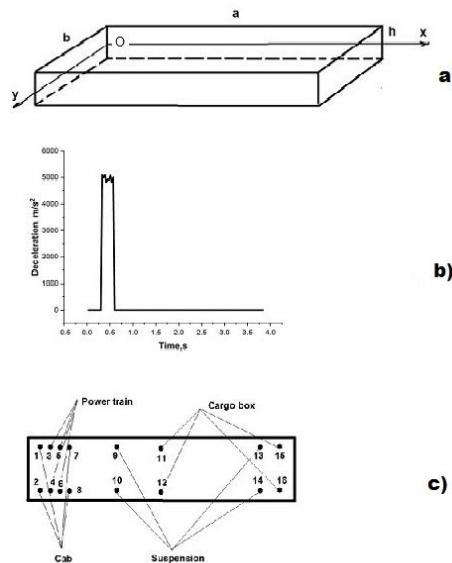
Figure 1. Idealized model of the vehicle frame 1a), vehicle deceleration during short-term braking 1b), and the position of the connection points of the engine, cabin, and cargo box 1c).

Illustration of the conection points is shown in Figure 1c), and the empirical coordinates of the points are given in Table 1.

Table 1. Coordinates of connection points

	Coordinate X, mm	Coordinate Y, mm
1	365	40
2	365	760
3	560	40
4	560	760
5	1375	40
6	1375	760
7	1496	40
8	1496	760
9	1600	40
10	1600	760
11	3400	40
12	3400	760
13	5015	40
14	5015	760
15	5050	40
16	5050	760

In order to determine the excitation forces, it was necessary to calculate the characteristic masses of the aggregates. This was done using statistical data on the percentage of aggregate masses in the vehicle mass, as well as based on recommendations for the size of the dead mass [2,3].

In addition to the mass of the aggregates and systems, it was necessary to calculate the distance between the supports along the length of the vehicle frame (which was done using data from Table 1) and define the height of the aggregate's center of gravity relative to the upper edge of the frame [1,3]. Approximate data is given in Table 2.

Table 2. Longitudinal distance of connection points, height of center of gravity relative to frame, and mass of aggregates and systems

	Connection point distance, mm	Center of gravity height, mm	Mass, kg
Power train	1010	200	962
Cab	1040	800	578
Cargo box	1915	850	890
Suspended mass	3600	1200	8070

The inertial force due to braking is given by the expression [2,3,5]:

$$F_i = m_i a,$$ (1)

where:

- a - decceleration defined by Figure 1b), and
- m_i - corresponding mass (power train, cab, cargo box, suspended mass).

We will assume that the center of mass of the aggregate and system is located in the middle of the longitudinal distance, so in that case, the static load (Fst) is equal on all mounts to a quarter of the gravitational force. The static force increases on the front mounts and decreases on the rear during vehicle braking. The magnitude of the force change due to braking is given by the expression [3,5]:

$$\Delta Z = \frac{F_i h_{ti}}{4 L_i} ,$$
(2)

where:

- F_i - inertial force due to braking, defined by equation (1),
- h_{ti} - height of the center of mass of the corresponding mass from Table 2,
- L_i - longitudinal distance between mounts from Table 2,
- + refers to the front, and - to the rear mounts.

Based on equations (1 and 2), the force on each mount is calculated [3]:

$$F = F_{st} \pm \Delta Z ,$$
(3)

Transverse vibrations of the elastic plate are described by a partial differential equation.The evalution of the partial differential equation that describes the transverse vibrations of the elastic plate is detailed in [3,6,7], it will not be done here, but only its final form will be presented [6]:

$$D\left(\frac{\partial^4 u}{\partial x^4} + 2\frac{\partial^4 u}{\partial x^2 \partial y^2} + \frac{\partial^4 u}{\partial y^4} \right) + \rho h \frac{\partial^2 u}{\partial t^4} = f\left(x,y,t\right),$$
(4)

where:

- u = u(x, y, t) - transverse vibrations of the frame,
- x - coordinate along the length of the frame,
- y - coordinate along the width of the frame,
- F(x, y, t) - disturbance transverse force (excitation function),
- t - time.

The value of D is given by the expression [6]:

$$D = \frac{Eh^3}{12\left(1-\upsilon^2\right)} ,$$
(5)

where:

- E - Young's modulus,
- υ -Poisson's ratio, and
- h - plate thickness.

As you know [6,7,8], in order to find the general integral of a partial differential equation (4), it is necessary to know the boundary and initial conditions.

In this specific case, all edges are free (torques and shear forces are equal to zero), and vibrations and their velocities are equal to zero at the initial time [3].

Mathematically, these conditions are defined by equations [3]:

$$M_x = -D\left(\frac{\partial^2 u}{\partial x^2} + \frac{\partial^2 u}{\upsilon \partial y^2}\right) = 0 : x = 0$$

$$V_x = Q_y - D\left[\frac{\partial^3 u}{\partial x^3} + \left(2 - \upsilon\right)\frac{\partial^3 u}{\partial x \partial y^2}\right] : x = 0; Q_y = 0$$

$$M_x = -D\left(\frac{\partial^2 u}{\partial x^2} + \frac{\partial^2 u}{\upsilon \partial y^2}\right) = 0 : x = a$$

$$V_x = Q_y - D\left[\frac{\partial^3 u}{\partial x^3} + \left(2 - \upsilon\right)\frac{\partial^3 u}{\partial x \partial y^2}\right] : x = a; Q_y = 0$$

$$M_y = -D\left(\frac{\partial^2 u}{\partial y^2} + \upsilon\frac{\partial^2 u}{\partial x^2}\right) = 0 : y = 0 \qquad\qquad (6)$$

$$V_y = Q_x - D\left[\frac{\partial^3 u}{\partial x^2 \partial y} + \left(2 - \upsilon\right)\frac{\partial^3 u}{\partial y^3}\right] : y = 0; Q_x = 0$$

$$M_y = -D\left(\frac{\partial^2 u}{\partial y^2} + \upsilon\frac{\partial^2 u}{\partial x^2}\right) = 0 : y = b$$

$$V_y = Q_x - D\left[\frac{\partial^3 u}{\partial x^2 \partial y} + \left(2 - \upsilon\right)\frac{\partial^3 u}{\partial y^3}\right] : y = b; Q_x = 0$$

$$u(x, y, 0) = 0$$

$$u`(x, y, 0) = 0$$

The disturbance force represents the sum of dynamic forces at the mounts [3]:

$$f(x, y, t) = \sum_{i=1}^{16} F_i(t), \qquad\qquad (7)$$

where the force Fi(t) is defined by expression (3) calculated at each mount.

The integral of the partial differential equation (4), with boundary, initial conditions (6), and disturbance force (7), can only be sought in the case of harmonic excitation (and not without difficulties), so an attempt was made to solve it using the Wolfram Mathematica 13.2 software [8]. However, this software allows solving partial differential equations up to the second order, so the problem had to be numerically solved [9] using the finite difference method.

The author developed software for solving the partial differential equation (4) using the finite difference method, with boundary, initial conditions (6), and disturbance force (7), in Pascal. It should be noted that in the case of numerical solving of partial differential equations, sometimes it is necessary to introduce additional boundary and initial conditions [8]..

2. VEHICLE FRAME DIMENSIONING

In the following text, there will be more words about optimal frame dimensioning, using optimization methods. It should be noted that various procedures are used in practice for this purpose, and here the method of "stochastic parametric optimization" will be applied. As known, the method of "stochastic parametric optimization" is used in the optimization of oscillatory parameters of motor vehicles and is based on nonlinear programming methods. Since there are constraints on design parameters in the optimization process, the problem is solved by introducing "external" or "internal" penalty functions [10,11].

In this specific case, the method of "stochastic parametric optimization" based on the Hooke-Jeeves method and "external" penalty functions was used for the selection of plate thickness (length and width are adopted). Considering that this optimization method is described in detail [10,11], it will not be done here. For illustration purposes, its block diagram will be shown in Figure 2, and the software is implemented in Pascal.

It was deemed appropriate to make the optimal choice of plate thickness (idealized frame) based on the conditions of minimal frame vibrations as an elastic system, its minimal mass, and maximum moment of inertia of the cross-section.
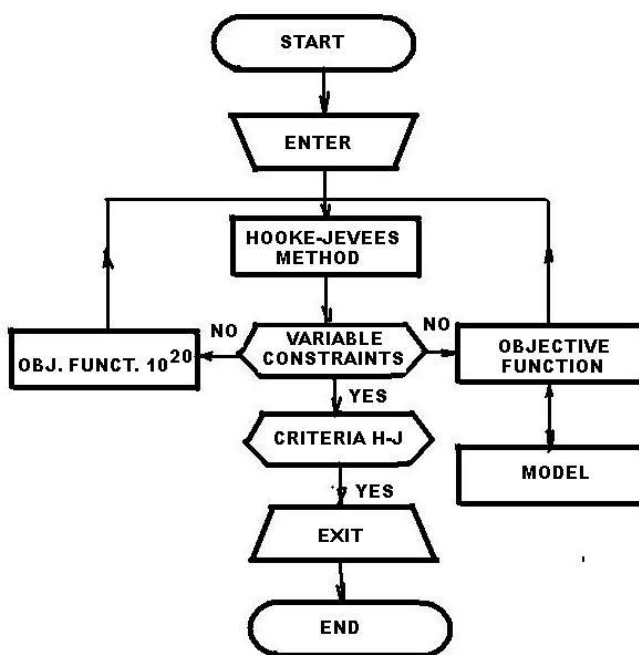
Figure 7. Block diagram of the used optimization method

Bearing this in mind, the objective function is used:

$$Z = r_1 u_{RMS} + r_2 m - r_3 I_x , \tag{8}$$

where:
- r_1, r_2, and r_3 - weighting factors that define the influence rank of sub-objectives in the objective function and allow the conversion of sizes defining sub-objectives into the same units (more words about their choice will be mentioned later),

- u_{RMS}- RMS values of frame vibrations obtained by solving the partial differential equation (4), and
- I_x - moment of inertia of the cross-section of the idealized frame.

The RMS of transverse frame vibrations is calculated using the expression:

$$u_{RMS}^2 = \frac{1}{n_x n_y n_t} \sum_{i=1}^{n_x} \sum_{j=1}^{n_y} \sum_{k=1}^{n_z} u(i,j,k)^2 , \qquad (9)$$

where:

- $u(i,j,k)$ - transverse vibrations of the idealized frame,
- n_x - number of points along the *x*-axis,
- n_y - number of points along the *y*-axis, and
- n_t - number of points along the *t*-axis.

The mass of the frame is calculated based on the dimensions of the cross-section and length, using the expression:

$$m = \rho b h l , \qquad (10)$$

where:

- b - width of the frame,
- h - thickness of the idealized frame,
- l - length of the frame, and
- ρ - density of the material.

The moment of inertia of the cross-section of the frame is calculated using the expression [12]:

$$I_x = \frac{bh^3}{12} , \qquad (11)$$

During the process of optimal selection of the thickness of the idealized frame, its boundary values are defined:

$$5 \leq h \leq 23 .$$

By introducing the optimizing parameter x[i], i=1(u-maximum, l-minimum), instead of h, with the corresponding adopted boundary values x_u[i], x_l[i], i=1, the objective function depends on one optimizing parameter, and it has multiple local minima and only one global minimum.

Considering that, in practice, the problem of finding the global minimum is solved by starting the optimization process with multiple initial values of the optimizing parameters [10,11], it was deemed appropriate to start with three initial values of these parameters, namely:

$$x = 0,5 x_u [1]$$

$$x = 0,8 x_u [1]$$

$$x = 1,2 x_l [1]$$

A dynamic simulation was performed for a steel frame structure with the following data: E=2.1*105, N/mm^2; ρ=8*10^{-6}, kg/mm^3; ν=0.3; n_x=128; n_y=128; n_t=128; h_x=47.65, mm; h_y=6.25, mm; h_t=0.08, s. The values of the number of points and discretization steps used during dynamic simulation ensured the reliability of the results for the parameter *x*: 0.00016 to 1.05, 1/mm, *y*: 0.0012 to 0.08, and *t*: 0.19 to 12.5 Hz [13].

Table 3. The data of the optimal selection of the thickness of the plate (idealized frame)

Initial values	Optimal parameter, h, mm	Objective function, Z, -	No of iter., N,-
0.5xu[i]	2.300000000000000E+001	-8.102355310777008E+005	1175
0.8(xu[i]) *	2.299999999999998E+001	-8.102355310776414E+005	863
1.2(xl[i]) *	2.299999999999988E+001	-8.102355310777E+005	567
0.5xu[i]**	5.000000000000192E+000	1.951759259703150E+002	484
0.8(xu[i]) **	5.000000209339827E+000	1.951759353878179E+002	746
1.2(xl[i]) **	5.00000000000021E+000	1.951759216328079E+002	273
0.5xu[i] ***	2.291000000000019E+001	1.576522170159383E-005	441
0.8(xu[i]) ***	1.853112842559817E+001	2.989550736588539E-005	206
1.2(xl[i]) ***	2.292999999999970E+001	1.572400545690352E-005	441
0.5xu[i] ****	2.298000000000023E+001	5.566501146807580E+005	443
0.8(xu[i]) ****	2.299773124575687E+001	5.543849553365553E+005	398
1.2(xl[i]) ****	2.299878906249978E+001	5.542498338388450E+005	436

Legend: $*r_1=1$; $r_2=1$; $r_3=1$; $** r_1=1$; $r_2=1$; $r_3=0$; $*** r_1=1$; $r_2=0$; $r_3=0$; $*** *r_1=3*1010$; $r_2=103$; $r_3=1$;

The optimization was performed on a Pentium 4 computer (Intel 2.4 GHz, 9 GB RAM), and the iterative process was automatically terminated when the difference between two adjacent values of the objective function was 10-15. The optimization time for each combination was about 25, minutes, and the calculated parameters are shown in Table 3.

3. DATA ANALYSIS

In order to select the ranks of influence on the objective function (Table 3), the optimization process was implemented with four groups. The first combination (*) introduced equal influence of sub-goals. However, the sub-goals did not have the same numerical values, so the moment of inertia had the greatest influence on the goal function, while the transverse vibrations had the smallest influence, which resulted in a negative sign in front of the numerical value of the objective function. Taking this into account, it was deemed appropriate to eliminate the influence of the moment of inertia from the objective function (combination **). Now, smaller values of the goal function have been obtained.

To determine how vibrations affect the goal function, research was conducted for combination (***). In this case, larger differences in the optimal thickness values were obtained, as well as differences in the minimum of the objective function.

Based on the aforementioned, the influence of the rank of influence and the type of sub-goal used on the process of optimal selection of plate thickness in the initial design phase of the frame is obvious and logical. Therefore, it was decided to give approximately equal influence to each individual sub-goal in expression (8). In this regard, a preliminary analysis was performed, and certain ranks of influence were marked with (****). Their application led to a change in the values of the goal function.

It can be concluded that the optimal plate thickness values are approximately equal, except in the case of (***). Namely, the optimal plate thickness is very close to its upper limit value. This can be explained by the fact that the used plate thickness interval is relatively small, and a larger thickness leads to a higher moment of inertia.

Therefore, it was considered appropriate to adopt a plate thickness of 22.99, mm as the optimal size (combination ****). It should be used to define the structure and dimensions of the ladder frame in the subsequent stages of vehicle design.

Having in mind what was previously said, it is appropriate in future research to start the optimization process with only one group of influence ranks, and that is in the middle of the interval.

In this case, the RMS vibration was $1.69381*10^{-5}$ mm, the mass was 897.41, kg, and the moment of inertia of cross-section was $8.10075*105$, $kgmm^4$.

It was deemed appropriate to examine the contribution of the calculated mass to the total mass of the newly designed vehicle (11000 kg). The obtained ratio was 8.15%, which can be considered acceptable for further project development [1,2,3].

It was deemed appropriate to perform an analysis of the transverse vibrations of the idealized frame for the optimal thickness. Considering that they depend on three parameters (*x, y, t*), which require the use of 4D graphics that do not exist in commercial form, it was deemed useful to use 3D graphics and only display vibrations for the centre of gravity planes, as illustrated in Figures 3 and 4.
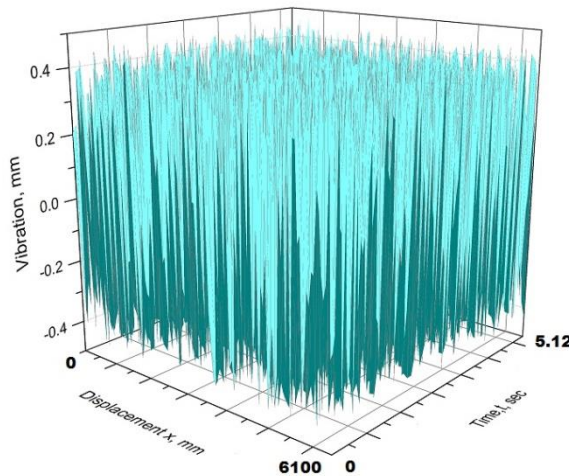
Figure 3. Transverse vibrations of the frame in the longitudinal center of gravity plane
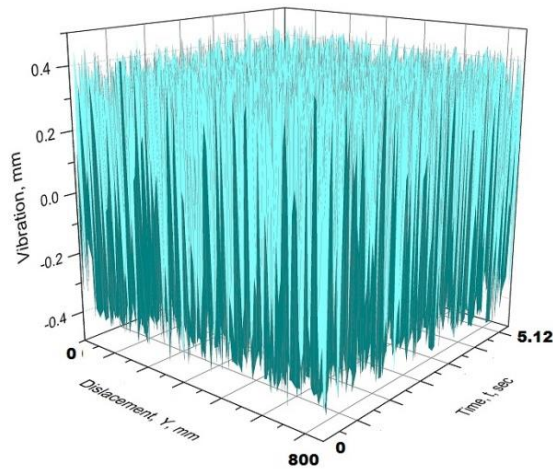
Figure 4. Transverse vibrations of the frame in the lateral center of gravity plane

From the analysis of the data from Figures 3 and 4, it can be determined that they vary stochastically along the length and width of the frame. The random nature of the vibrations can be explained by the random nature of the excitation force used, and the change in vibrations across the surface of the plate is in accordance with [6,7,14].

It was deemed appropriate to perform a frequency analysis of the transverse vibrations using 3D Fourier transform, using a program developed in Pascal. For the same reasons as in the previous case, the results are only shown for the center of gravitty planes, in Figures 5-8.
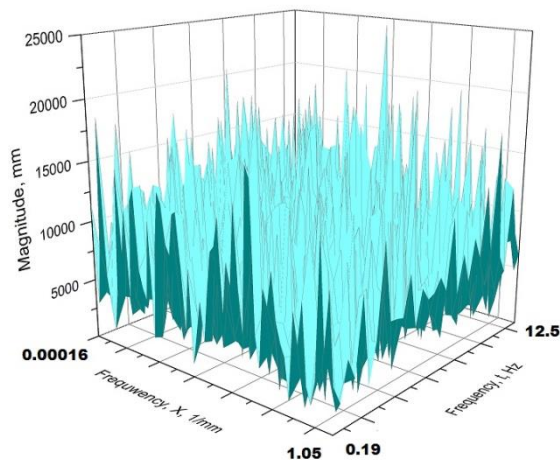
Figure 5. Spectrum magnitude of frame vibrations in the longitudinal center of gravity plane

Contribution to the development of a method for optimal dimensioning of the frame in the initial design phase of a heavy motor vehicle

37
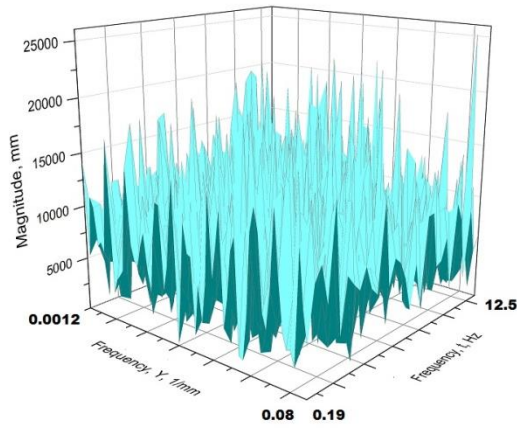
Figure 6. Spectrum magnitude of the frame in the lateral center of gravity plane
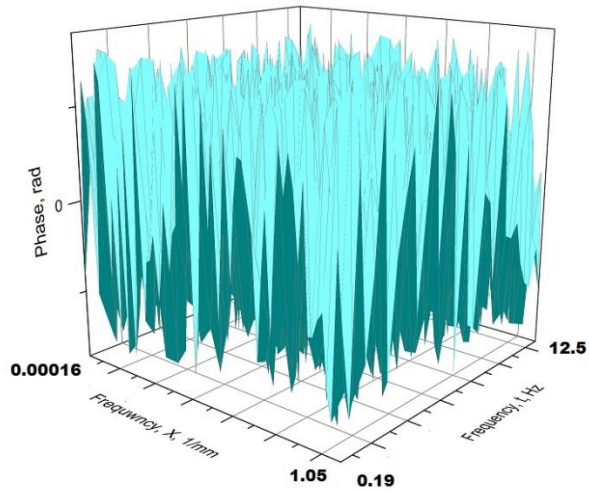
Figure 7. Phase angles of the vibration spectrum of the frame in the longitudinal center of gravity plane
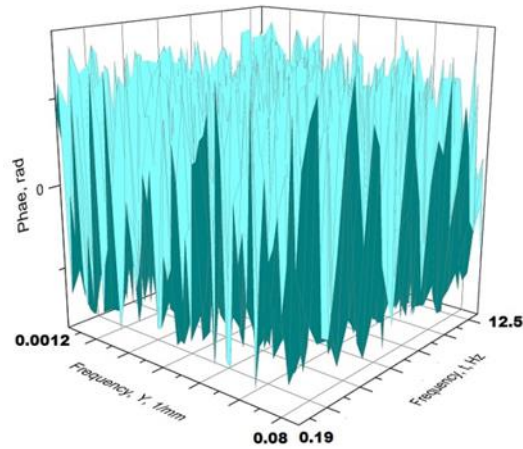
Figure 8. Phase angles of the vibration spectrum of the frame in the lateral center of gravity plane

Note that the calculated plate thickness is approximate and may be subject to change during the structural verification using finite element method and experimentation, which will not be discussed here [4].

It should also be noted that there are no explicit procedures for calculating errors in spectral analysis for 3D Fourier transform, as in the case of 1D Fourier transform [10]. Considering this, as well as the fact that the goal of this study is to illustrate the potential application of 3D Fourier transform in the analysis of transverse vibrations of the vehicle frame, statistical errors were not calculated...

4. CONCLUSIONS

In conclusion, the developed procedure, based on the analysis of transverse vibrations, mass, and moment of inertia cross-section of the vehicle frame, allows for the definition of its dimensions in the initial phase of vehicle design.

In further development of the project, based on these defined parameters, more detailed calculations can be performed, potentially using the finite element method.

The conducted analyses have shown that the use of 3D Fourier transform is desirable for the analysis of transverse vibrations of the vehicle frame..

REFERENCES

[1]   Demić, M.: Basics of designing heavy motor vehicles, Faculty of Mechanical Engineering in Kragujevac, 1994 (in Serbian).
[2]   Simić, D.: Motor vehicles, Scientific book, Belgrade, 1988 (in Serbian).
[3]   Demić, M. Development of a method for defining the torsional stiffness of the frame in the initial phase of designing a heavy motor vehicle, Mobility and Vehicle Mechanics, Vol 49, No 3, pp. 15-29, https://doi.org/10.24874/mvm.2023.49.03.02 (2023).

Intentionally blank

[4]   Bathe, K.J. : Finite Element Procedures in Engineering Analyses, Prentice Hall, Englewood Cliffs, N.J, 1982.

[5]   Gillespie, T.: Fundamementals of Vehicle Dynamics, SAE,1992.

[6]   Singeresy, S.R. : Vibration of continuous systems, John Wiley and Sons, Inc. New Jersey, 2007.

[7]   Sobolev, S. L.: Partial differential equations of Mathematical Physics, Pergamon Student Edition, Elsevier, 2016.

[8]   Wolfram   Mathematica: https://Reference.Wolfram.com/language/tutorial/NDSolverPDE.html

[9]   Stanton, R. G.L: Numerical methods for Science and Engineering, Prentice Hall, Englewood Cliffs, N.J,1961.

[10] Bunday P.: Basic optimization methods. Spottiswoode Ballantyne, Colchester and London, 1984.

[11] Demić M.: Optimization of vehicles elastodamping elements Characteristics from the aspect of ride comfort, Vehicle System Dynamics, Vol. 23 , No 5, pp 351-370, 1994.

[12] Timoshenko, S.: Strength of materials, Part II, Advanced Theory and Problems, Paolo Atto, California, 1941.

[13] Bendat, J.S., Piersol, A.G.: Random Data-Analysis and measurement procedures, John Wiley and Sons, 2000

[14] Demić, M.: Application of multi-parameter frequency analysis in experimental identification of vibration parameters in motor vehicles, Mobility and Vehicle Mechanics, Vol. 49, No. 1, pp 25-37, https://doi.org/10.24874/mvm.2023.49.01.03 (2023).

A TWO-STAGE MODEL FOR ELECTRIC VEHICLE EVALUATION: CRITIC-ELECTRE APPROACH

Danijela Tadić [1]*, Jovanka Lukić[2], Nikola Komatina[3]

ABSTRACT: Sustainable development represents one of the primary strategic management challenges for organizations operating across various economic sectors. The production and utilization of transportation means aimed at reducing greenhouse gas emissions lead to an enhancement of environmental protection. Many automotive companies are deploying electric vehicles, thus contributing to sustainable development. However, selecting the most suitable electric vehicle from the available options poses a challenge. This paper aims to introduce a two-stage model that integrates the CRiteria significance Through Intercriteria Correlation and Elimination (CRITIC) method with ÉLimination Et Choix Traduisant la REalité (ELECTRE). The CRITIC method is used to obtain weighs vector of electric vehicle attributes, while the ELECTRE method is used for ranking the considered electric vehicle models. The proposed model is demonstrated using a sample of 17 feasible electric vehicle variants, evaluated based on seven features. Input data are sourced from relevant literature. The novelty of this research lies in the combined CRITIC-ELECTRE approach, which has not been previously applied in this domain.

KEY WORDS: *Electric vehicles, CRITIC, ELECTRE*

[1]*Danijela Tadić, Faculty of Engineering, University of Kragujevac, Sestre Janjic 6, Kragujevac, Serbia, galovic@kg.ac.rs, https://orcid.org/0000-0003-2236-967X (*Corresponding author)*
[2] *Jovanka Lukić, Faculty of Engineering, University of Kragujevac, Sestre Janjic 6, Kragujevac, Serbia, lukicj@kg.ac.rs, https://orcid.org/0000-0002-5893-3976*
[3] *Nikola Komatina, Faculty of Engineering, University of Kragujevac, Sestre Janjic 6, Kragujevac, Serbia, nkomatina@kg.ac.rs, https://orcid.org/0000-0001-6964-5673*

DVOSTEPENI MODEL OCENJIVANJA ELEKTRIČNIH VOZILA: CRITIC-ELECTRE PRISTUP

Danijela Tadić, Jovanka Lukić, Nikola Komatina

REZIME: Održivi razvoj predstavlja jedan od primarnih izazova strateškog upravljanja za organizacije koje posluju u različitim privrednim sektorima. Proizvodnja i korišćenje transportnih sredstava u cilju smanjenja emisije gasova staklene bašte dovode do unapređenja zaštite životne sredine. Mnoge automobilske kompanije koriste električna vozila i na taj način doprinose održivom razvoju. Međutim, izbor najpogodnijeg električnog vozila među dostupnim opcijama predstavlja izazov. Ovaj rad ima za cilj da uvede dvostepeni model koji integriše metodu značajnosti kriterijuma kroz međukriterijumsku korelaciju i eliminaciju (CRITIC) sa ELimination Et Choik Traduisant la REalite (ELECTRE). Metoda CRITIC se koristi za dobijanje vektora težine atributa električnih vozila, dok se metoda ELECTRE koristi za rangiranje razmatranih modela električnih vozila. Predloženi model je demonstriran na uzorku od 17 varijanti električnih vozila, procenjenih na osnovu sedam karakteristika. Ulazni podaci su dobijeni iz relevantne literature. Novina ovog istraživanja leži u kombinovanom pristupu CRITIC-ELECTRE, koji do sada nije primenjivan u ovoj oblasti.

KLJUČNE REČI: *Električno vozilo, CRITIC, ELECTRE*

A TWO-STAGE MODEL FOR ELECTRIC VEHICLE EVALUATION: CRITIC-ELECTRE APPROACH

Danijela Tadić, Jovanka Lukić, Nikola Komatina

INTRODUCTION

These days, one of the most crucial tasks for logistic managers in industrial organizations is to develop a well-defined sustainable transport system. This is aimed at minimizing environmental problems and resource depletion, and this objective is understood in a broader sense. Additionally, it should aim to maximize social and economic welfare (1). Batery Electric Vehicles (BEVs) hold significant potential for advancing sustainable transport, primarily due to their relatively high efficiency and the potential to operate independently from unsustainable energy sources (2). Some authors (3), (4) argue that electric vehicles (EVs) possess several advantages, including efficient battery capacity, reduced emissions of hazardous gases, government subsidies and other incentives for purchases, enhanced vehicle performance, and various other environmental benefits. Based on the findings of the study by (5), it can be concluded that BEVs exhibit up to a 70% lower environmental impact compared to diesel vehicles. However, customer demand for BEVs primarily depends on support measures, such as financial incentives (6).

Many automotive companies have begun developing various models of BEVs with diverse features. These features aim to satisfy the dynamic demands of customers, as highlighted by (7). Numerous studies in the relevant literature focus on measuring customer preferences for BEV selection. For instance, (8) consider BEV features such as battery capacity, charging time, driving range, and acceleration. Some authors argue that it's essential to consider factors like style, colour, quality, size, and performance of BEVs (9).

According to (10) the battery is a crucial component of an BEV, and the car's success largely depends on battery technology, which impacts driving range, recharging time, acceleration, and cost savings. They identify battery capacity, seating capacity, driving range, price, torque, acceleration, charging time, and charging infrastructure as the most important EV features. Similarly, (9) also consider various BEV features such as driving range, price, battery capacity, charging time, seating capacity, and torque.

Therefore, evaluating and selecting the most suitable BEV model while considering various features is a challenging task for customers. This problem can be framed as a multi-attribute decision-making (MADM) task.

In MADM problems, determining weights is a critical issue that can significantly influence the final outcome. Over the last few decades, researchers worldwide have focused their attention on addressing this problem. Most authors suggest dividing the model for determining criteria weights into subjective and objective approaches (11). Subjective approaches reflect the personal assessments of decision makers (DMs), which are based on their knowledge, experience, and intuition. In the literature, the Analytic Hierarchy Process (AHP) (12) is the most commonly used subjective MADM method for determining weights. On the other hand, CRiteria significance Through Intercriteria Correlation (CRITIC) (13) is one of the most well-known and frequently used objective methods. This MADM method belongs to the category of correlation methods, which utilize the standard deviations of the elements of the normalized decision matrix and the correlation coefficients of all pairs of attributes.

The ranking problem can be addressed by applying numerous MADM methods, which can be classified into different groups (14). There are no recommendations or rules on how to choose an MADM method for determining the rank of alternatives. This decision can be considered a problem in itself and Depends on the Assessments of DMs. In (15) a detailed review of the literature on the application of MADM techniques in various research domains is provided. To determine the stability of solutions, many authors use two or more MADM methods (16), (17).

In the relevant literature, several papers address the problem through two-stage models integrating two or more MADM methods (3), (18),(9). In the initial stage, weights of electric vehicle (EV) features are determined using the Analytic Hierarchy Process (AHP) (3), (9). Subsequently, in the second stage, various other MADM methods are employed to ascertain the ranking of EVs. For example, the Multi-Attributive Border Approximation Area Comparison (MABAC) method developed by (19) is utilized in (3) and (9), while the ELimination Et Choix Traduisant la REalité (ELECTRE) method developed by (20) is employed in (18).

When comparing papers that propose models for ranking EV models, certain differences can be observed and further described. This analysis also highlights the advantages of the proposed model.

In (3), five BEV features were considered, determined based on DMs' assessments. In (17) conducted a detailed literature review on the number and models of EV features described in relevant literature. This author suggests 14 EV features. In (9) defined a list of EV features based on research results. Firstly, they made a shortlist of BEV features from past academic literature based on subjective assessments. Secondly, they conducted a survey involving customers who already use BEVs or intend to buy them in the future. Customers expressed their assessments of the importance of BEV features. Pareto analysis was used to shortlist the most significant criteria (9). This list contains 6 EV features. Therefore, it can be considered that the BEV features obtained in the exact manner (9) are more reliable than in other papers found in the relevant literature. In this research, the authors expanded the list of BEV features defined in (9). The authors believe that the considered EV models can be adequately assessed respecting the seven features.

In papers (3), (9), the weight vector of BEV features is determined using AHP. This approach means that the calculated weights of EV features are influenced by the subjective opinions of DMs. In this research, the CRITIC method was used to determine BEV features weights as in (21). The authors believe that: (i) the sample of considered EVs is sufficiently large and (ii) the values of elements in the decision matrix are obtained from literature sources, so the applied statistical data analysis is reliable. In other words, the obtained values of EV feature weights by applying CRITIC are sufficiently accurate.

The rank of considered BEVs is determined by MABAC in (9), (3). By applying the MABAC method, all types of BEVs are divided into two groups. BEV models belonging to the upper approximation area can adequately meet customer demand, while those in the lower approximation area are undesirable from the customers' perspective. In (18) classified BEV models using ELECTRE, as in this research. In papers found in the literature, the normalized decision matrix is constructed by applying different normalization procedures (18),(22). In this research, the procedure of enhanced normalization (23), is used. The introduced modifications of the ELECTRE method do not compromise the rigor of the research according to the authors' opinions.

The paper is organized as follows. The proposed integrated multi-attribute model for the evaluation and selection of BEVs is presented in Section 2. Section 3 provides a test and verification of the proposed model using real-life data. Concluding remarks and directions for future research are discussed in Section 4.

1   METHODOLOGY

The evaluation and ranking of EVs are conducted through a two-stage MADM model. In the first stage, the weights of EV features used to evaluate EV models are determined using CRITIC. In the second stage, the ranking of EVs is obtained by applying ELECTRE.

1.1 Defining set of EV models

The share of small and medium electric car models is decreasing among available BEV models. In 2023, two-thirds of the battery-electric models on the market were SUVs 5 pick-up trucks or large cars. Just 25% of BEV car sales in the United States were for small and medium models, compared to 40% in Europe and 50% in China. EVs are following the same trend as conventional cars, and getting bigger on average. In 2023, SUVs, pick-up trucks and large models accounted for 65% of total ICE vehicle sales worldwide, and more than 80% in the United States, 60% in China and 50% in Europe (24).

In Emerging Market and Developing Economies (EMDEs), the absence of small and cheaper EV models is a significant hindrance to wider market uptake. Many of the available BEV models are SUVs or large models, targeting consumers of high-end goods, and far too expensive for mass-market consumers, who often do not own a personal vehicle in the first place.

In EMDEs, some EV can be cheaper than ICE equivalents over their lifetime. Access to finance is typically much more challenging in EMDEs due to higher interest rates and the more limited availability of cheap capital. Passenger EV have also a significantly lower market penetration in the first place, and many car purchases are made in second-hand markets.

Achieving price parity between electric and ICE cars will be an important tipping point. Even when the TCO for electric cars is advantageous, the upfront retail price plays a decisive role, and mass-market consumers are typically more sensitive to price premiums than wealthier buyers. This holds true not only in EMDEs, which have comparatively high costs of capital and comparatively low household and business incomes, but also in advanced economies. In the United States, for example, surveys suggest affordability was the top concern for consumers considering EV adoption in 2023. Other estimates show that even among SUV and pick-up truck consumers, only 50% would be willing to purchase one above USD 50 000.

Larger batteries for longer ranges increase car prices, equipment, digital technology and luxury features that are often marketed on top of the base model. A disproportionate focus on larger, premium models is pushing up the average price, which added to the lack of available BEV models in second-hand markets limits potential to reach mass-market consumers. Importantly, geopolitical tension, trade and supply chain disruptions, increasing battery prices in 2022 relative to 2021, and rising inflation, have also significantly affected the potential for further cost declines (24).

The "city" group consists of compact vehicles with a universal character, mostly for daily urban but also extra-urban driving as well as most everyday applications. The "small"

segment includes cars with small dimensions, practically suitable only for urban driving, as their range does not allow for a longer trip without the need for additional charging.

Over the past years, BEVs has gained increasing attention by policymakers and consumers, especially due to their potential to reduce Green House Gasses (GHG) emissions. Thus, electric vehicle market has been shown significant growth in today. Many Famous manufacturers have converted to electrical concept the vehicle portfolio of themself. There are many electric vehicle models and firms that are present in market with different combinations. So, many car manufacturers have started to the development studies on BEVs for better performance and this process continues rapidly. However, BEVs have some disadvantage, existing limitations and difference to each other such as limited driving ranges, insufficient chargers, long recharging duration and upfront purchasing cost. These differences show varies according to automobile company and automobile types. Besides, BEVs make a significant contribution sustainability in terms of environmental effect in cities. To do this, BEVs as cleaner technology should be supported by decision makers, and all society. While technical aspects are very relevant for the successful introduction of these new vehicles, to decide for the best automobile among alternatives need multi-criteria evaluation process. When a customer needs to acquire a new electric auto-mobile or automobile for its daily life, many factors must be taken into account. This requires a good command of conflicting factors, which can benefit from the domain of Multi-Criteria Decision Making (MCDM). There are various factors which affect the performance of an electric vehicle such as battery capacity, charging time, price, driving range etc. All these factors are improved further by manufacturers day by day. So, the BEV technology has been getting momentum rapidly every passing day. These differences and limitations of BEVs have been necessitated the decision-making process for purchase preferences of customers. In addition, we will find the answer to the question of which vehicle is the most suitable or optimal with this study, we will help to customers for their purchase preference with analytic and optimization models. The effective selection of electric automobile for multiple criteria types is essential for the sustainable practice of trans-portation. Besides, when the problem has got constraints and goal values, mathematical models such as goal programming (GP) give optimal results.

In general, it is possible to consider various types of electric vehicles I which are formally represented by a set of indices $\{1,..,i,..,I\}$. The index of electric vehicles is denoted as i, where $i = 1,..,I$. This paper considers the following types of electric vehicles: Fiat 500 e hatchback 42 kWh ($i = 1$), Renault 5 E Tech 52 kWh 150hp ($i = 2$), Renault ZOE ZE50 R110 ($i = 3$), Lancia Ypsilon ($i = 4$), Renault ZOE ZE50 R135 ($i = 5$), Renault ZOE ZE50 R135 ($i = 6$), Mini Cooper SE ($i = 7$), Renault 5 E Tech 40 kWh 150hp ($i = 8$), Opel Corsa electric 50 kWh ($i = 9$), Peugeot e-208 51 kWh ($i = 10$), Opel Corsa electric 51 kWh ($i = 11$), Mini Cooper E ($i = 12$), Renault 5 E-Tech 40 kWh 120 hp ($i = 13$), Fiat 500 e hatchback 24 kWh ($i = 14$), Fiat 500e 3+1 42 kWh ($i = 15$), Abarth 500e Hatchback ($i = 16$), and Abarth 500e Convertible ($i = 17$) which are collected in May 2024.

1.2 Defining EV Features

In general, each type of EV can be evaluated based on K features. These attributes are formally represented by a set of indices $\{1,..,k,..,K\}$. The index of a feature is denoted as k, where $k = 1,..,K$. In this research, features are defined by decision makers based on the results of the study (9) and the best practices. These features are: driving range (measured in kilometres) ($k = 1$), price (measured in euros) ($k = 2$), nominal battery capacity (measured in kWh) ($k = 3$), usable battery capacity (measured in kWh) ($k = 4$), charging time

(measured in hours) ($k = 5$), seating capacity (number of passengers) ($k = 6$), and torque (measured in Nm) ($k = 7$).

1. 3 Determining the weight vector of EV features based on CRITIC

The proposed algorithm can be implemented through the following steps, as outlined below:

Step 1. The decision matrix is stated:

$$\left[x_{ik} \right]_{lxK}, \tag{1}$$

The values of elements x_{ik} are obtained based on empirical data.

Step 2. The normalized decision matrix is constructed using the Linear Normalization Procedure (25), as proposed in conventional CRITIC.

$$\left[r_{ik} \right]_{IxK}, \tag{2}$$

where:

$$r_{ik} = \frac{x_{ik}}{\sum_{i=1,\ldots,l} x_{ik}}. \tag{3}$$

Step 3. Determine weights of EV features, $W_k, k = 1,..,K$ according to formula:

$$W_k = \sigma_k \sum_{k=1,\ldots,K} \left(1 - \rho_{kk`} \right). \tag{4}$$

where:

- σ_k is standard deviation values for each EV feature $k, k = 1,..,K$
- $\rho_{kk'}$ is the correlation coefficient between each pair of EV features.

Step 4. The normalized weights vector of EV features is denoted as:

$$\left[\omega_k \right]_{Kx1}, \tag{5}$$

where:

$$\omega_k = \frac{W_k}{\sum_{i=1,\ldots,K} W_k}. \tag{6}$$

1.4 Ranking of EVs based on ELECTRE

Step 1. The decision matrix is stated:

$$\left[x_{ik} \right]_{IxK}, \tag{7}$$

The values of elements x_{ik} are obtained based on empirical data.

Step 2. The normalized decision matrix is constructed using the enhanced normalization method (26):

$$\left[r_{ik} \right]_{IxK}, \tag{8}$$

where:

a) benefit type

$$r_{ik} = 1 - \frac{x_k^{max} - x_{ik}}{\sum_{i=1}^{l}\left(x_k^{max} - x_{ik}\right)} . \tag{9}$$

b) cost type

$$r_{ik} = 1 - \frac{x_{ik} - x_k^{min}}{\sum_{i=1}^{I}\left(x_{ik} - x_k^{min}\right)}$$

$$x_k^{max} = \max_{i=1,...,I} x_{ik} \tag{10}$$

$$x_k^{min} = \min_{i=1,...,I} x_{ik}$$

Step 3. The weighted normalized decision matrix is constructed in this way:

$$\left[z_{ik}\right]_{IxK} , \tag{11}$$

where:

$$z_{ik} = \omega_k \cdot r_{ik} , \tag{12}$$

Step 4. Determine the concordance sets, $S_{ii'}$ and discordance sets, $NS_{ii'}$:

$$z_{i`k} \geq z_{ik} \rightarrow k \in S_{ii`}$$
$$z_{i`k} < z_{ik} \rightarrow k \in NS_{ii`} \tag{13}$$

Step 5. The concordance matrix is constructed:

$$\left[c_{ii`}\right]_{IxI} , \tag{14}$$

where:

$$c_{ii`} = \sum_{k=1,...,K`} \omega_k . \tag{15}$$

The concordance level is calculated as:

$$\bar{c} = \frac{1}{I \cdot (I-1)} \sum_{i=1,...,I} \sum_{i`=1,...,I} c_{ii`} . \tag{16}$$

Step 6. The discordance matrix is constructed:

$$\left[n_{ii`}\right]_{IxI} , \tag{17}$$

where:

$$n_{ii`} = \frac{\max_{k \in NS_{ii`}}|z_{i`k} - z_{ik}|}{\max_{k=1,...,K}|z_{i`k} - z_{ik}|} . \tag{18}$$

The disconcordance level is calculated as:

$$\bar{n} = \frac{1}{I \cdot (I-1)} \sum_{i=1,\ldots,I} \sum_{i`=1,\ldots,I} n_{ii`} \,. \tag{19}$$

Step 7. To construct the general matrix based on Boolean matrices, we first create Boolean matrices using a minimum concordance level and a minimum discordance level:

2   CASE STUDY

In this section, the proposed methodology is illustrated using real-life data. The section is divided into two parts. In the first part, the proposed CRITIC method is applied to obtain the weights vector of criteria. In the second part, the ranking of the considered EV models is determined using the proposed ELECTRE method.

2. 1 An application of CRITIC

The attribute values for each considered type of BEV are provided based on literature sources and presented in Table 1 (Step 1 of the proposed algorithm).

Table 1. Decision matrix

	$k = 1$	$k = 2$	$k = 3$	$k = 4$	$k = 5$	$k = 6$	$k = 7$
$i = 1$	235	34990	42	37.3	4	4	220
$i = 2$	330	32000	55	52	5.75	5	245
$i = 3$	315	36840	54.7	52	3	5	225
$i = 4$	305	40000	51	48.1	5.25	5	260
$i = 5$	310	37840	54.7	52	3	5	245
$i = 6$	290	37475	50	46.3	7.3	5	260
$i = 7$	310	36900	54.2	49	5.25	4	330
$i = 8$	260	25000	43	40	4.5	5	215
$i = 9$	295	34650	50	46.3	7.5	5	260
$i = 10$	310	40325	51	48.1	7.75	5	260
$i = 11$	315	38045	51	48.1	7.75	5	260
$i = 12$	235	32900	40.7	37	4	4	290
$i = 13$	260	28000	43	40	4.5	5	225
$i = 14$	135	30990	23.8	21.3	2.3	4	220
$i = 15$	235	36990	42	37.3	4	4	220
$i = 16$	225	37990	42.2	37.8	4.25	4	235
$i = 17$	225	40990	42.2	37.8	4.25	4	235

The normalized decision matrix (Step 2 of the proposed algorithm) is constructed, and the standard deviation of criteria values is determined. These values are presented in Table 2.

Table 2. The normalized decision matrix

	$k = 1$	$k = 2$	$k = 3$	$k = 4$	$k = 5$	$k = 6$	$k = 7$
$i = 1$	0.054	0.058	0.053	0.051	0.047	0.051	0.052
$i = 2$	0.076	0.053	0.070	0.071	0.068	0.064	0.058
$i = 3$	0.072	0.061	0.069	0.071	0.036	0.064	0.054
$i = 4$	0.070	0.066	0.065	0.066	0.062	0.064	0.062
$i = 5$	0.071	0.063	0.069	0.071	0.036	0.064	0.058
$i = 6$	0.067	0.062	0.063	0.063	0.087	0.064	0.062
$i = 7$	0.071	0.061	0.069	0.067	0.062	0.051	0.078
$i = 8$	0.060	0.042	0.054	0.055	0.053	0.064	0.051
$i = 9$	0.068	0.058	0.063	0.063	0.089	0.064	0.062
$i = 10$	0.071	0.067	0.065	0.066	0.092	0.064	0.062
$i = 11$	0.072	0.063	0.065	0.066	0.092	0.064	0.062
$i = 12$	0.054	0.055	0.051	0.051	0.047	0.051	0.069
$i = 13$	0.060	0.047	0.054	0.055	0.053	0.064	0.054
$i = 14$	0.031	0.051	0.030	0.029	0.027	0.051	0.052
$i = 15$	0.054	0.061	0.053	0.051	0.047	0.051	0.052
$i = 16$	0.052	0.063	0.053	0.052	0.050	0.051	0.056
$i = 17$	0.052	0.068	0.053	0.052	0.050	0.051	0.056
σ_k	0.012	0.007	0.010	0.011	0.020	0.007	0.007

The normalized weight vector of the considered attributes is obtained by applying the proposed algorithm (Step 3 to Step 4), so that:

$$\omega = [0.112 \quad 0.142 \quad 0.096 \quad 0.105 \quad 0.299 \quad 0.117 \quad 0.129]$$

2. 3 An application of ELECTRE

The decision matrix is shown in Table 1. The normalized decision matrix (Step 2 of the proposed algorithm) is presented in Table 3.

Table 3 The normalized decision matrix

	$k = 1$	$k = 2$	$k = 3$	$k = 4$	$k = 5$	$k = 6$	$k = 7$
$i = 1$	0.899	0.941	0.910	0.904	0.962	0.857	0.915
$i = 2$	1	0.959	1	1	0.924	1	0.934
$i = 3$	0.984	0.930	0.998	1	0.985	1	0.917
$i = 4$	0.974	0.912	0.972	0.975	0.935	1	0.946
$i = 5$	0.979	0.924	0.998	1	0.985	1	0.934
$i = 6$	0.958	0.926	0.965	0.963	0.889	1	0.946
$i = 7$	0.979	0.930	0.994	0.980	0.935	0.857	1
$i = 8$	0.926	1	0.917	0.922	0.951	1	0.911
$i = 9$	0.963	0.943	0.965	0.963	0.885	1	0.946
$i = 10$	0.979	0.910	0.972	0.975	0.880	1	0.946
$i = 11$	0.984	0.923	0.972	0.975	0.880	1	0.946
$i = 12$	0.899	0.953	0.899	0.902	0.962	0.857	0.969
$i = 13$	0.926	0.982	0.917	0.922	0.951	1	0.917
$i = 14$	0.794	0.965	0.784	0.800	1	0.857	0.915
$i = 15$	0.899	0.929	0.910	0.904	0.962	0.857	0.915
$i = 16$	0.889	0.923	0.911	0.908	0.957	0.857	0.926
$i = 17$	0.889	0.906	0.911	0.908	0.957	0.857	0.926

By applying the proposed algorithm (Step 4), the weighted normalized decision matrix is obtained and presented in Table 4.

Table 4 The weighted normalized decision matrix

	$k = 1$	$k = 2$	$k = 3$	$k = 4$	$k = 5$	$k = 6$	$k = 7$
$i = 1$	0.101	0.134	0.087	0.095	0.288	0.100	0.118
$i = 2$	0.112	0.136	0.096	0.105	0.276	0.117	0.120
$i = 3$	0.110	0.132	0.096	0.105	0.295	0.117	0.118
$i = 4$	0.109	0.130	0.093	0.102	0.280	0.117	0.122
$i = 5$	0.110	0.131	0.096	0.105	0.295	0.117	0.120
$i = 6$	0.107	0.131	0.093	0.101	0.266	0.117	0.122
$i = 7$	0.110	0.132	0.095	0.103	0.280	0.100	0.129

$i = 8$	0.104	0.142	0.088	0.097	0.284	0.117	0.118
$i = 9$	0.108	0.134	0.093	0.101	0.265	0.117	0.122
$i = 10$	0.110	0.129	0.093	0.102	0.263	0.117	0.122
$i = 11$	0.110	0.131	0.093	0.102	0.263	0.117	0.122
$i = 12$	0.101	0.135	0.086	0.095	0.288	0.100	0.125
$i = 13$	0.104	0.139	0.088	0.097	0.284	0.117	0.118
$i = 14$	0.089	0.137	0.075	0.084	0.299	0.100	0.118
$i = 15$	0.101	0.132	0.087	0.095	0.288	0.100	0.118
$i = 16$	0.100	0.131	0.087	0.095	0.286	0.100	0.119
$i = 17$	0.100	0.129	0.087	0.095	0.286	0.100	0.119

Determining the sets of concordance and discordance (Step 4 of the proposed algorithm) is illustrated by example:

$$S_{12} = \{k = 1, k = 2; k = 3; k = 4; k = 6; k = 7\}$$

In a similar manner, all sets of concordance and discordance for each pair of considered BEVs are determined.

$$c_{12} = 0.112 + 0.142 + 0.096 + 0.105 + 0.117 + 0.129 = 0.70$$

$$n12 = \frac{\max(0.012)}{\max(0.011, 0.002, 0.009, 0.010, 0.012, 0.017, 0.002)} = \frac{0.012}{0.017} = 0.71$$

In a similar manner, the remaining values of the concordance matrix and discordance matrix are determined, which are presented in Table 5 and Table 6, respectively.

Table 5 The concordance matrix

-	0.30	0.27	0.44	0.14	0.44	0.56	0.43	0.44	0.44	0.44	0.73	0.43	0.56	1	0.87	0.87
0.70	-	0.70	0.57	0.70	0.87	0.57	0.56	0.87	0.87	0.87	0.57	0.56	0.56	0.70	0.70	0.70
0.86	0.62	-	0.87	0.81	0.87	0.87	0.86	0.73	0.87	0.87	0.73	0.86	0.56	1	0.87	0.87
0.56	0.55	0.25	-	0.25	0.86	0.42	0.61	0.86	0.89	0.75	0.43	0.56	0.56	0.56	0.56	0.70
0.86	0.75	0.86	0.87	-	0.87	0.73	0.86	0.73	0.87	0.87	0.73	0.86	0.56	0.86	1	1
0.56	0.25	0.25	0.48	0.39	-	0.12	0.56	0.75	0.78	0.78	0.43	0.56	0.56	0.56	0.70	0.70
0.56	0.43	0.38	0.88	0.38	0.88	-	0.44	0.74	0.88	0.88	0.56	0.44	0.56	0.70	0.70	0.70
0.70	0.56	0.39	0.56	0.26	0.56	0.56	-	0.56	0.56	0.56	0.57	1	0.70	0.70	0.57	0.57
0.70	0.25	0.39	0.48	0.39	0.70	0.26	0.56	-	0.78	0.78	0.43	0.56	0.56	0.70	0.70	0.70
0.56	0.25	0.36	0.56	0.36	0.56	0.23	0.56	0.56	-	0.86	0.43	0.56	0.56	0.56	0.56	0.70
0.56	0.25	0.36	0.70	0.50	0.70	0.23	0.56	0.56	1	-	0.43	0.56	0.56	0.56	0.70	0.70

0.90	0.43	0.27	0.57	0.27	0.57	0.56	0.43	0.57	0.57	0.57	-	0.43	0.44	0.90	0.90	0.90
0.70	0.56	0.39	0.44	0.26	0.56	0.56	0.86	0.57	0.56	0.56	0.57	-	0.70	0.70	0.57	0.57
0.69	0.44	0.57	0.44	0.44	0.44	0.56	0.43	0.44	0.44	0.44	0.56	0.43	-	0.69	0.56	0.56
0.90	0.30	0.27	0.44	0.14	0.44	0.56	0.43	0.30	0.44	0.44	0.73	0.43	0.56	-	0.87	0.87
0.45	0.30	0.13	0.44	0.14	0.44	0.42	0.43	0.30	0.44	0.44	0.32	0.43	0.56	0.45	-	1
0.45	0.30	0.13	0.30	0.30	0.30	0.42	0.43	0.30	0.44	0.30	0.32	0.43	0.56	0.45	0.86	-

$$\bar{c} = \frac{1}{17 \cdot 16} \cdot 156.818 = 0.58$$

Table 6 The disconcordance matrix

-	1	1	1	1	0.77	1	0.77	0.68	0.68	1	0.29	1	1	0	0.5	0.2
0.71	-	1	0.67	1	0.20	0.53	1	0.18	0.15	0.15	0.71	1	1	0.71	0.59	0.59
0.12	0.21	-	0.27	1	0.14	0.65	0.91	0.13	0.12	0.12	0.41	0.64	0.24	0	0.06	0.06
0.47	1	1	-	1	0.07	0.41	1	0.27	0.06	0.06	0.47	1	0.95	0.47	0.35	0.35
0.18	0.26	0.50	0.13	-	0.07	0.53	1	0.10	0.06	0.06	0.29	0.73	0.29	0.06	0	0
1	1	1	1	1	-	0.82	1	1	1	1	1	1	1	1	1	1
0.73	1	1	1	1	1	-	1	1	1	1	0.89	1	0.90	0.73	0.60	0.60
1	1	1	0.42	1	0.28	0.65	-	0.26	0.29	0.29	0.41	0	0.88	0.24	0.12	0.12
1	1	1	1	1	0.33	0.88	1	-	0.40	0.67	1	1	1	1	1	1
1	1	1	1	1	1	1	1	1	-	1	1	1	1	1	1	1
0.14	1	1	1	1	1	1	1	1	0	-	1	1	1	1	1	1
1	1	1	1	1	0.77	1	1	0.74	0.68	0.68	-	1	0.92	0.14	0.14	0.17
0.92	1	1	0.56	1	0.28	0.65	1	0.26	0.29	0.29	0.41	-	0.88	0.24	0.12	0.12
0	1	1	1	1	0.55	1	1	0.56	0.58	0.50	1	1	-	1	0.92	0.92
1	1	1	1	1	0.77	1	1	0.74	0.68	0.68	1	1	0.92	-	0.50	0.33
1	1	1	1	1	0.85	1	1	0.81	0.74	0.74	1	1	1	1	-	0
1	1	1	1	1	0.85	1	1	0.81	0.74	0.74	1	1	1	1	1	-

$$\bar{n} = \frac{1}{17 \cdot 16} \cdot 202.869 = 0.75$$

According to the defined rules (Step 7 of the proposed algorithm), the concordance dominance matrix is determined and presented in Table 7.

Table 7 The general matrix

-	0	0	0	0	0	0	0	0	0	0	1	0	0	1	1	1
1	-	0	0	0	1	0	0	1	1	1	0	0	0	1	1	1
1	1	-	1	0	1	1	0	1	1	1	1	1	0	1	1	1
0	0	0	-	0	1	0	0	1	1	1	0	0	0	0	0	1
1	1	1	1	-	1	1	0	1	1	1	1	1	0	1	1	1
0	0	0	0	0	-	0	0	0	0	0	0	0	0	0	0	0

0	0	0	0	0	0	-	0	0	0	0	0	0	0	1	1	1
0	0	0	0	0	0	0	-	0	0	0	0	1	0	1	0	0
0	0	0	0	0	1	0	0	-	1	1	0	0	0	0	0	0
0	0	0	0	0	0	0	0	0	-	0	0	0	0	0	0	0
0	0	0	0	0	0	0	0	0	1	-	0	0	0	0	0	0
0	0	0	0	0	0	0	0	0	0	0	-	0	0	1	1	1
0	0	0	0	0	0	0	0	0	0	0	0	-	0	1	0	0
1	0	0	0	0	0	0	0	0	0	0	0	0	-	0	0	0
0	0	0	0	0	0	0	0	0	0	0	0	0	0	-	1	1
0	0	0	0	0	0	0	0	0	0	0	0	0	0	0	-	1
0	0	0	0	0	0	0	0	0	0	0	0	0	0	0	0	-

By applying the proposed procedure (Step 7 to Step 8), the determined values are presented in Table 8.

Table 8 Rank of considered BEVs

	M_i	rank		M_i	rank
$i = 1$	4	5	$i = 10$	0	15-17
$i = 2$	8	3	$i = 11$	1	11-14
$i = 3$	13	2	$i = 12$	3	6-8
$i = 4$	5	4	$i = 13$	1	11-14
$i = 5$	14	1	$i = 14$	1	11-14
$i = 6$	0	15-17	$i = 15$	2	9-10
$i = 7$	3	6-8	$i = 16$	1	11-14
$i = 8$	2	9-10	$i = 17$	0	15-17
$i = 9$	3	6-8			

Based on the obtained ranking, it is evident that all considered BEVs can be divided into 9 groups. In the first place, i.e. second place in the rank, we have the Renault ZOE ZE50 R135, i.e. the Renault ZOE ZE50 R110, respectively. It can be considered that these two types of BEVs are the best with respect to all BEV characteristics as well as their weights. The obtained result can be beneficial for customers to make decisions more easily. For BEV manufacturers, these results should enable designers, production managers, and sales managers to benchmark and thus improve their products.

CONCLUSIONS

The demands for strong competition require the automotive strategic management team to define, implement, and monitor a strategy constructed based on changes in customer preferences. It is believed that stricter environmental regulations will lead to increased usage of BEVs. In this paper, the problem of evaluating and ranking small BEVs most commonly used in the worldwide markets is considered.

The first novelty lies in the method used for rating the relative importance of criteria. CRITIC does not involve cumbersome mathematical operations. This characteristic of CRITIC is important when the dimensions of the problem under consideration are large. The application of the CRITIC method enables objective determination of criteria weights, thereby reducing the burden of subjective assessments by DMs and ensuring greater accuracy.

The second novelty is the ranking of BEV models performed using the proposed ELECTRE method. A modification of conventional ELECTRE has been made in the domain of constructing the normalized decision matrix. In conventional ELECTRE methods, linear

normalization is applied without considering the type of criterion. In this research, the authors used an enhanced normalization method with respect to criterion type. This increased the complexity of calculating the normalized decision matrix. However, the authors believe that the applied normalization procedure is more suitable for the problem under consideration. On the other hand, the complexity of computation in subsequent steps is significantly reduced. It can be considered that the modification of ELECTRE reduces computational complexity on one hand while increasing the accuracy of the obtained results on the other hand.

By using the ELECTRE method, many BEV models are placed at the same rank position. Through the application of the ELECTRE method, all considered BEV models are grouped into several groups. Therefore, it can be concluded that this MADM method is highly useful for solving the considered problem.

The advantages of the proposed two-stage MADM compared to models found in the literature include: (i) consideration of criteria weights obtained accurately, (ii) ranking of BEV models determined by the proposed ELECTRE on a sufficiently large sample, and (iii) application of the proposed two-stage MADM for improving the development strategy of BEVs in the automotive industry.

The proposed method is flexible in accommodating changes in the number of criteria, the number of BEV models, and adjustments to criteria weights.

However, the proposed model has certain constraints. The main constraints include the selection of BEV models and defining features of BEVs that meet customer demand.

Future research directions involve analysing the robustness of solutions when changing the method for determining criteria weights. Additionally, the proposed model can be extended to analyse other management decision problems in various research areas.

In theoretical terms, future research should include sensitivity analysis of the obtained solution when criteria weights are determined using subjective methods or different normalization procedures. In practical terms, future research involves developing a software solution that would facilitate the user-friendly application of the proposed two-stage model for strategic management of automotive companies.

AKNOWLEDGEMENT

REFERENCES

1. Zhao X, Ke Y, Zuo J, Xiong W, Wu P. Evaluation of sustainable transport research in 2000–2019. J Clean Prod. 2020;256:120404.
2. Borén S, Nurhadi L, Ny H, Robèrt KH, Broman G, Trygg L. A strategic approach to sustainable transport system development - Part 2: the case of a vision for electric vehicle systems in southeast Sweden. J Clean Prod. 2017;140:62–71.
3. Biswas TK, Das MC. Selection of Commercially Available Electric Vehicle using Fuzzy AHP-MABAC. Vol. 100, Journal of The Institution of Engineers (India): Series C. Springer; 2019. p. 531–7.
4. Langbroek JHM, Franklin JP, Susilo YO. The effect of policy incentives on electric vehicle adoption. Energy Policy. 2016;94:94–103.

5. Gustafsson M, Svensson N, Eklund M, Fredriksson Möller B. Well-to-wheel climate performance of gas and electric vehicles in Europe. Transp Res Part D Transp Environ. 2021;97:102911.

6. Francisco S, Mock P, Yang Z. DRIVING ELECTRIFICATION A GLOBAL COMPARISON OF FISCAL INCENTIVE POLICY FOR ELECTRIC VEHICLES. 2014.

7. Zarazua de Rubens G, Noel L, Kester J, Sovacool BK. The market case for electric mobility: Investigating electric vehicle business models for mass adoption. Energy. 2020;194:116841.

8. Das MC, Pandey A, Mahato AK, Singh RK. Comparative performance of electric vehicles using evaluation of mixed data. OPSEARCH. 2019;56(3):1067–90.

9. Sonar HC, Kulkarni SD. An Integrated AHP-MABAC Approach for Electric Vehicle Selection. Res Transp Bus Manag. 2021;41:100665.

10. Dijk M, Orsato RJ, Kemp R. The emergence of an electric mobility trajectory. Energy Policy. 2013;52:135–45.

11. Zhu G-N, Hu J, Qi J, Gu C-C, Peng Y. An integrated AHP and VIKOR for design concept evaluation based on rough number. Adv Eng Informatics. 2015;29:408–18.

12. Saaty TL. How to make a decision: The analytic hierarchy process. Eur J Oper Res. 1990;48(1):9–26.

13. Diakoulaki D, Mavrotas G, Papayannakis L. Determining objective weights in multiple criteria problems: The critic method. Comput Oper Res. 1995;22(7):763–70.

14. Zayat W, Kilic HS, Yalcin AS, Zaim S, Delen D. Application of MADM methods in Industry 4.0: A literature review. Comput Ind Eng. 2023;177:109075.

15. Aleksić A, Tadić D. Industrial and Management Applications of Type-2 Multi-Attribute Decision-Making Techniques Extended with Type-2 Fuzzy Sets from 2013 to 2022. Mathematics. 2023;11(10).

16. Komatina N, Djapan M, Ristić I, Aleksić A. Fulfilling External Stakeholders' Demands—Enhancement Workplace Safety Using Fuzzy MCDM. Sustainability. 2021;13(5).

17. Ziemba P. Selection of electric vehicles for the needs of sustainable transport under conditions of uncertainty—a comparative study on fuzzy mcda methods. Energies. 2021 Nov 1;14(22).

18. Romero-Ania A, Rivero Gutiérrez L, De Vicente Oliva MA. Multiple Criteria Decision Analysis of Sustainable Urban Public Transport Systems. Mathematics. 2021;9(16).

19. Pamučar D, Ćirović G. The selection of transport and handling resources in logistics centers using Multi-Attributive Border Approximation area Comparison (MABAC). Expert Syst Appl. 2015;42(6):3016–28.

20. Roy B. The Outranking Approach and the Foundations of Electre Methods. In: e Costa CA, editor. Readings in Multiple Criteria Decision Aid. Berlin, Heidelberg: Springer Berlin Heidelberg; 1990. p. 155–83.

21. Rostamzadeh R, Ghorabaee MK, Govindan K, Esmaeili A, Nobar HBK. Evaluation of sustainable supply chain risk management using an integrated fuzzy TOPSIS-CRITIC approach. J Clean Prod. 2018 Feb 20;175:651–69.

22. Daneshvar Rouyendegh B, Erman Erkan T. SELECTION OF ACADEMIC STAFF USING THE FUZZY ANALYTIC HIERARCHY PROCESS (FAHP): A PILOT

STUDY. Teh Vjesn. 2012;19:923–9.

23.   Zhou P, Ang BW, Poh KL. Comparing aggregating methods for constructing the composite environmental index: An objective measure. Ecol Econ. 2006 Sep 20;59(3):305–11.

24.   Energy Agency I. Global EV Outlook 2024 Moving towards increased affordability. 2024.

25.   GARDZIEJCZYK W, ZABICKI P. Normalization and variant assessment methods in selection of road alignment variants – case study. J Civ Eng Manag. 2017 Apr 21;23(4):510–23.

26.   Jahan A, Edwards KL. A state-of-the-art survey on the influence of normalization techniques in ranking: Improving the materials selection process in engineering design. Mater Des. 2015;65:335–42.

Intentionally blank

IMPACT OF MICROSTRUCTURED SURFACE ON THE FATIGUE PERFORMANCE OF POLYPROPYLENE SPECIMENS FOR ADVANCED HYDROGEN AUTOMOTIVE APPLICATIONS

Krisztián Kun [1]*, Adrián Bognár[2], Bence Molnár[3]

ABSTRACT: The automotive industry is increasingly focusing on lightweight and high-performance materials to meet stringent environmental and efficiency standards. Polymers play a pivotal role in this shift, as they offer design flexibility and significant weight reduction. Injection moulding is one of the most widely used manufacturing processes for producing high-quality plastic components in the automotive sector. A critical application area is in hydrogen fuel cell vehicles, where the integrity and durability of Type 4 hydrogen storage tanks depend on the strong adhesion between the polymer liner and the composite structure. Enhancing this bond is crucial to ensuring safety and performance under high-pressure conditions. By tailoring the surface microstructure of polymer liners through advanced injection moulding techniques, the adhesion to composite materials can be significantly improved. Despite the detailed mechanical properties provided in the technical data sheets of polymers, fatigue characteristics are often not included, even though many automotive plastic components are exposed to repetitive stresses during their operational life. This research aims to investigate the effect of microstructures created by modern manufacturing technology, which is currently undergoing significant development for automotive applications, particularly in relation to hydrogen technology.

---

[1]*Krisztián Kun, Department of Innovative Vehicles and Materials, GAMF Faculty of Mechanical Engineering and IT, John von Neumann University, H-6000 Kecskemét, Hungary;
kun.krisztian@nje.hu, ⊙ https://orcid.org/0000-0001-7194-3581 (*Corresponding author)*
[2]*Adrián Bognár, Department of Innovative Vehicles and Materials, GAMF Faculty of Mechanical Engineering and IT, John von Neumann University, H-6000 Kecskemét, Hungary;
bognar.adrian@nje.hu,*
[3]*Bence Molnár, Department of Innovative Vehicles and Materials, GAMF Faculty of Mechanical Engineering and IT, John von Neumann University, H-6000 Kecskemét, Hungary;
molnar.bence@nje.hu, ⊙ https://orcid.org/0009-0001-8410-8814*

UTICAJ MIKROSTRUKTURISANE POVRŠINE NA OTPORNOST NA ZAMOR POLIPROPILENSKIH UZORAKA ZA NAPREDNE AUTOMOBILSKE PRIMENE U HIDROGENSKOJ TEHNOLOGIJI

REZIME: Automobilska industrija sve više se fokusira na lake materijale visokih performansi kako bi ispunila stroge standarde ekologije i efikasnosti. Polimeri igraju ključnu ulogu u ovoj tranziciji, jer omogućavaju fleksibilnost u dizajnu i značajno smanjenje težine. Brizganje plastike je jedan od najčešće korišćenih proizvodnih procesa za izradu visokokvalitetnih plastičnih komponenti u automobilskoj industriji. Ključna oblast primene je u vozilima sa vodoničnim gorivnim ćelijama, gde integritet i izdržljivost vodoničnih rezervoara tipa 4 zavise od jake adhezije između polimerne obloge (liner) i kompozitne strukture. Poboljšanje ove veze je presudno za obezbeđivanje bezbednosti i performansi u uslovima visokog pritiska. Prilagođavanjem mikrostrukture površine polimernih obloga primenom naprednih tehnika brizganja, adhezija sa kompozitnim materijalima može se značajno poboljšati. Iako tehnički podaci polimera obuhvataju detaljne mehaničke karakteristike, osobine zamora često nisu uključene, iako su mnoge plastične komponente u automobilima izložene ponavljajućim naprezanjima tokom svog radnog veka. Ova istraživanja imaju za cilj da ispitaju uticaj mikrostruktura stvorenih savremenim proizvodnim tehnologijama, koje trenutno prolaze kroz značajan razvoj za primene u automobilskoj industriji, posebno u vezi sa vodoničnom tehnologijom.

KLJUČNE REČI: *Zamor, mikrostruktura, femtosekundni laser, tip 4*

IMPACT OF MICROSTRUCTURED SURFACE ON THE FATIGUE PERFORMANCE OF POLYPROPYLENE SPECIMENS FOR ADVANCED HYDROGEN AUTOMOTIVE APPLICATIONS

Krisztián Kun, Adrián Bognár, Bence Molnár

INTRODUCTION

The automotive industry is undergoing a transformative shift towards sustainable and efficient energy solutions, with hydrogen technology emerging as a key player in the pursuit of zero-emission vehicles [1-3]. Hydrogen fuel cells offer a promising alternative to traditional combustion engines and battery-electric vehicles, providing high energy density and rapid refuelling capabilities [4-6]. However, the successful integration of hydrogen technology in automotive applications is heavily dependent on the development of reliable and durable storage systems, such as Type 4 hydrogen tanks (**Figure 1**), which utilize a polymer liner reinforced with composite materials. Kis et al. (2023) emphasized the importance of strong adhesion between the polymer liner and the composite shell to prevent structural failures under high-pressure conditions [7]. Surface modifications at the microstructural level have been shown to significantly enhance the mechanical interlocking and adhesion properties of polymer composites. Berczeli (2018) demonstrated that advanced surface modification techniques could improve the adhesion strength between polymers and composite materials, making them suitable for high-stress environments like hydrogen storage systems [8]. Furthermore, Weltsch and colleagues, in their 2023 study, found that femtosecond laser ablation can precisely control the microstructure of the polymer surface, optimizing the interface between the liner and the composite. This approach not only enhances adhesion but also contributes to improved fatigue resistance [9]. Fatigue performance is a critical factor in the long-term reliability of polymer components in automotive applications. S. Mortazavian et al. highlighted that while the mechanical properties of polymers are well-documented, their fatigue characteristics are often neglected [10]. This oversight is particularly significant in automotive applications where parts are exposed to repetitive stresses, such as in hydrogen storage systems. Ahmadifar et al., in their publication, pointed out that understanding the fatigue behaviour of polymer components is essential for ensuring the safety and durability of hydrogen-powered vehicles [11].

This study aims to build on the existing body of research by investigating the effect of microstructured surfaces on the fatigue behaviour of polypropylene specimens, a widely used polymer in automotive applications. By examining different microstructural configurations and their impact on mechanical properties, this research seeks to provide insights into the optimization of polymer components for advanced hydrogen automotive applications.

Figure 1. A Type 4 tank (JEC World 2022) - own photo.

1. MATERIALS AND METHODS

The rapid expansion of plastics in various fields, particularly in automotive and aerospace industries, is notable. Despite their growing use, our understanding of the material characteristics of polymers is less comprehensive compared to metals. Engineering plastics are well-defined in terms of properties like tensile strength, elongation, and Young's modulus. However, their resistance to cyclic loading, or fatigue behavior, is less explored. This is especially critical as many plastic components are subjected to repetitive mechanical stress during their service life, impacting their longevity and performance. Consequently, accurate and reliable methods to determine these characteristics are essential for modern research. Fatigue in polymers involves cyclic stresses that are often below the material's yield strength, leading to failure over time. These failures can be classified into low-cycle fatigue, characterized by a combination of elastic and plastic deformation, and high-cycle fatigue, which occurs under primarily elastic conditions. Unlike metals, which exhibit a constant modulus of elasticity within their elastic limit, polymers demonstrate higher internal damping and lower thermal conductivity. This results in significant heating of the specimen under cyclic loading, even at low frequencies. The increase in temperature can cause a reduction in modulus, affecting the material's mechanical properties and performance. Moreover, polymers, especially in additive manufacturing [12],[13] do not have a well-defined fatigue limit as seen in metals. Instead, fatigue testing for polymers is typically conducted up to a certain number of cycles - often 10^7 cycles - to determine the corresponding stress levels under specific conditions like frequency, temperature, and humidity. Despite this, comprehensive and standardized methods for assessing fatigue behavior in polymers are lacking. Current practices primarily rely on data provided by material manufacturers, with limited empirical validation. As a result, there is a pressing need for systematic and thorough research to develop reliable fatigue characterization methods for polymers, particularly for applications that require high mechanical performance under cyclic loading [14]. Addressing this knowledge gap is crucial for advancing the use of polymers in critical applications, such as automotive components and hydrogen storage systems, where reliable material performance is essential. Establishing robust testing methods and understanding the underlying mechanisms of polymer fatigue will enable the development of more durable and efficient components, meeting the increasing demands of modern engineering applications. [11]

For this research, a special injection moulding tool was used, which produces two standard bending test specimens. Our goal was to create microstructures on the surface of the stationary mould insert that would have varying effects on the melt flow during the injection process. To influence the polymer melt, grooves were formed both perpendicular and parallel to the flow direction. In injection moulding, the mould cavity is filled by a complex, expansive flow, which results in the formation of a shell-core structure that varies depending on the process parameters. This study aims to investigate the influence of microstructures formed on the mould surface on the fatigue performance of different test specimens. The microstructures generated on the mould surface can directly impact the internal material structure of the moulded product and indirectly affect the bonding strength of associated elements, such as composite layers. Understanding these effects is crucial for optimizing the mechanical properties and durability of injection-moulded components, particularly in applications requiring high-performance materials.

1.1 FATIGUE TEST EQUIPMENT

The fatigue testing machine (**Figure 2**) operates on the principle of resonance, meaning that the test specimen, along with the attached clamping part, forms an oscillating system within the testing machine. This setup allows for precise replication of cyclic loading conditions, ensuring that the frequency of the machine corresponds exactly to the natural frequency of the test specimens. The machine mechanically transfers the applied load to the test specimen, simulating real-world fatigue conditions. This method is highly effective for studying the fatigue behavior of materials under controlled and repeatable conditions, which is essential for developing accurate fatigue life predictions. The polymer fatigue testing machine at the John von Neumann University is designed by Sebők and Fodor [15]. The device is designed to accommodate standard tensile test specimens, which means that, according to the task requirements, standard workpieces will need to be produced and tested to carry out fatigue testing and measurements.
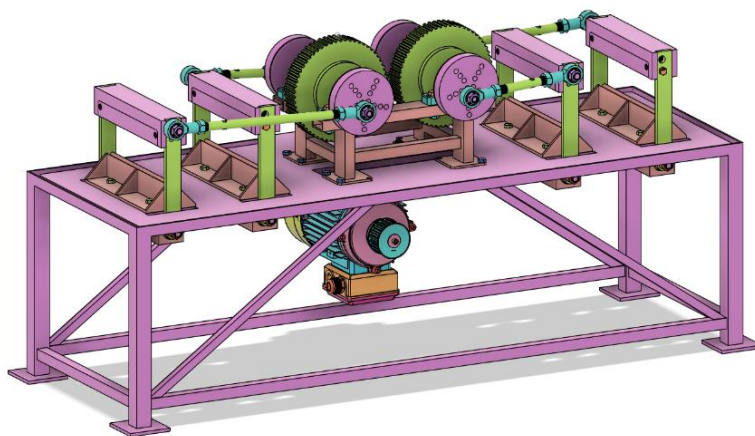

Figure 2. The fatigue testing machine.

1.2 LASER STRUCTURED INJECTION MOULDING CAVITY

The process was carried out using a Monaco 1035-80-40 industrial femtosecond laser equipped with a LINOS F-Theta-Ronar scanning optics system and a focal length lens of f = 254 mm. The power laser was calibrated based on the literature [8],[9], aiming to achieve a microstructure depth capable of influencing the polymer flow during injection moulding. Such as pulse energy and scanning speed can precisely control the depth and shape of microstructures, impacting the flow behaviour and, consequently, the mechanical properties of the final product.

Creating grooves on the mould surface that are parallel or perpendicular to the polymer melt flow could potentially have distinct effects on the final properties of the moulded product (**Figure 3**). Grooves aligned parallel to the flow direction might streamline the flow, potentially reducing turbulence and leading to a more uniform alignment of polymer chains along the flow. This alignment could enhance properties such as tensile strength and stiffness in that direction. Conversely, grooves oriented perpendicular to the flow might introduce disruptions in the polymer alignment, which could potentially increase shear forces and promote a more complex internal structure. This disruption might improve the material's resistance to crack propagation and increase its toughness.
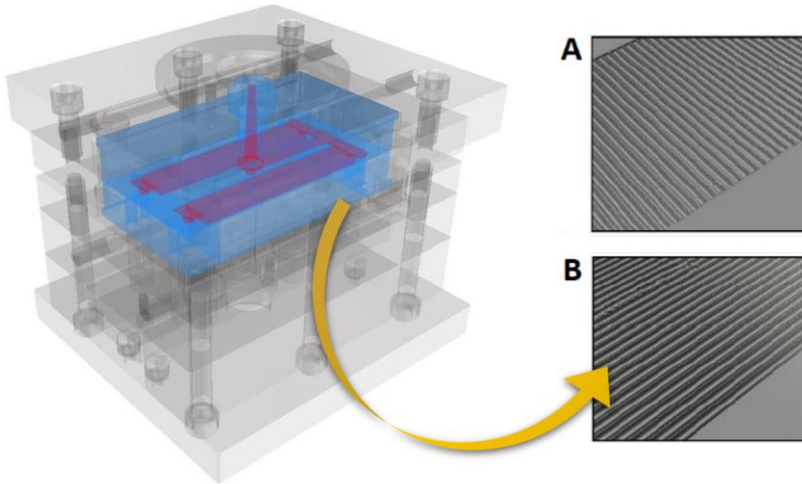
Figure 3. The injection moulding tool and its microstructured cavity: A – perpendicular, B – parallel to the flow front.

After creating micro-grooves oriented both parallel and perpendicular to the melt flow direction on the mould cavity surface (**Figure 4**), the treated area was analysed with a Keyence VHX-2000 digital microscope to verify the groove depth. The analysis revealed an average depth of 83 μm. This depth was observed both in the surface-treated parts parallel and perpendicular to the direction of flow.

Figure 4. A microscopic image of the cavity surface with dimensions.

1.3 POLYPROPYLENE RAW MATERIAL

The selection of the base material was influenced by its suitability for technical applications and favourable manufacturing properties. Polypropylene (PP) was chosen, specifically a thermoplastic random copolymer known as Tatren RM 85 82 Clear. This material is characterized by its high flowability and excellent processing stability. According to its technical datasheet, it can be processed efficiently using conventional injection moulding machines at temperatures ranging from 190 to 230 °C. The test specimens were produced following the recommended processing parameters outlined in the datasheet [16], ensuring optimal material performance and consistency during manufacturing.

2. ANALYSIS

The applied test specimens were selected based on the results of the initial bending tests. The testing frequency was set to 5 Hz, as recommended in the literature [15]. In the first phase, the specimens were subjected to 1,000 cycles, followed by 10,000 cycles in the second phase, 100,000 cycles in the third, and 1,000,000 cycles in the final phase. The bending amplitude used during testing was 10 mm. All fatigue tests were conducted at room temperature. During the fatigue testing (**Figure 5**), the specimens were monitored using a thermal camera to observe temperature changes. The desired bending amplitude was achieved by adjusting the eccentric discs mounted on the transmission shafts, allowing precise control over the mechanical loading conditions.

To establish a reference for the effect of the structured surfaces, test specimens were also produced using an untreated mould insert with a ground surface. This allowed for direct comparison between the structured and non-structured surfaces, providing a baseline to evaluate the influence of the microstructures on the mechanical properties and behaviour of the specimens. 25 samples per type were compared.

Figure 5. In-process photo of the fatigue test.

3. RESULTS AND DISCUSSION

In the earlier tests at 1,000, 10,000, and 100,000 cycles, all specimens exhibited similar flexural strength, showing no significant differences in performance (Figure 6). However, at the one million cycle test, only the specimens with parallel microstructures were able to retain their initial flexural strength values, while those with other structures showed a decline. This suggests that the alignment of polymer chains along the parallel grooves enhances load distribution and reduces stress concentrations during extended cyclic loading.
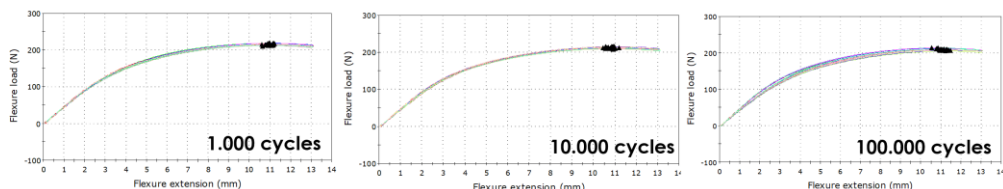

Figure 6. Flexural Strength Comparison of Specimens after 1000, 10 000, and 100 000 Cycles.
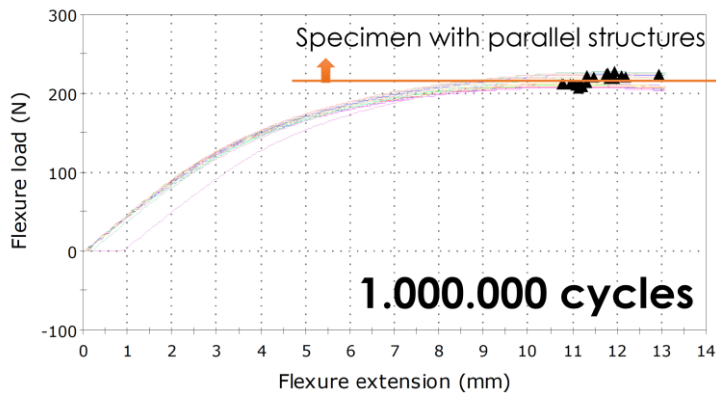
Figure 7. Flexural Strength Retention of Parallel and Perpendicular Microstructures after One Million Cycles.

The measured difference in flexural strength between the parallel structures and the perpendicular or ground surfaces ranged from 5 to 8%. This suggests that the parallel microstructures are more effective in maintaining the material's mechanical properties over extended fatigue testing (**Figure 7**). Their ability to align polymer chains along the groove direction likely contributes to better stress distribution and reduced strain concentration, which helps prevent early strength degradation compared to the other surface configurations.

AKNOWLEDGEMENT

REFERENCES

[1]   Maghrour Zefreh Mohammad, Adam Torok. Theoretical Comparison of the effects of different traffic conditions on urban road environmental external costs. Sustainability March 2021; 13:3541. https://doi.org/10.3390/su13063541

[2]   Vodovozov Valery, Raud Zoja, Petlenkov Eduard. Review of energy challenges and horizons of hydrogen city buses. Energies September 2022; 15:6945. https://doi.org/10.3390/en15196945

[3]   Wróbel Kamil, et al. Hydrogen internal combustion engine vehicles: a review. Energies November 2022; 15:8937. https://doi.org/10.3390/en15238937

[4]   Fan Lixin, Tu Zhengkai, Chan Siew Hwa. Recent development of hydrogen and fuel cell technologies: a review. Energy Rep November 2021; 7:8421e46. https://doi.org/10.1016/j.egyr.2021.08.003

[5]   Manoharan Yogesh, et al. Hydrogen fuel cell vehicles; current status and future prospect. Appl Sci June 2019; 9:2296. https://doi.org/10.3390/app9112296 [Online].

[6]   Ioan-Sorin Sorlei, et al. Fuel cell electric vehicles – a brief review of current topologies and energy management strategies. Energies January 2021;14:252. https://doi.org/10.3390/en14010252

[7] Kis, Dávid István, and Eszter Kókai. "A review on the factors of liner collapse in type IV hydrogen storage vessels." *International Journal of Hydrogen Energy* (2023). https://doi.org/10.1016/j.ijhydene.2023.09.316

[8] Berczeli, M., and Z. Weltsch. "Improvement of adhesive joining of hybrid aluminum–GFRP using surface modifications." *IOP Conference Series: Materials Science and Engineering*. Vol. 448. No. 1. IOP Publishing, 2018. https://doi.org/10.1088/1757-899X/448/1/012050

[9] Weltsch, Zoltan, Ferenc Tajti, and Miklós Berczeli. "Development of the bonding technology of modern automotive materials with environmentally friendly solutions." *KOMUNIKACIE/COMMUNICATIONS* 26.2 (2024): B135-B141. https://doi.org/10.26552/com.C.2024.026

[10] Mortazavian, S., and A. Fatemi. "Tensile and fatigue behaviors of polymers for automotive applications: Zähigkeits-und Ermüdungsverhalten von Polymeren für Automobilanwendungen." *Materialwissenschaft und Werkstofftechnik* 46.2 (2015): 204-213. https://doi.org/10.1002/mawe.201400376

[11] Ahmadifar, Mohammad, et al. "Exploring fatigue characteristics of metallic boss-polymer liner adhesion in hydrogen storage tanks: Experimental insights post surface treatment." *Journal of Energy Storage* 75 (2024): 109771. https://doi.org/10.1016/j.est.2023.109771

[12] Azadi, M., et al. "High-cycle bending fatigue properties of additive-manufactured ABS and PLA polymers fabricated by fused deposition modeling 3D-printing." *Forces in Mechanics* 3 (2021): 100016. https://doi.org/10.1016/j.finmec.2021.100016

[13] Safai, Lauren, et al. "A review of the fatigue behavior of 3D printed polymers." *Additive manufacturing* 28 (2019): 87-97. https://doi.org/10.1016/j.addma.2019.03.023

[14] Guo, Rui, et al. "The fatigue performances of carbon fiber reinforced polymer composites–a review." *Journal of Materials Research and Technology* 21 (2022): 4773-4789. https://doi.org/10.1016/j.jmrt.2022.11.053

[15] Fodor, Antal, and Pál Boza. "Designing Fatigue Experiment for Investigating Polymer Specimens." *MACRo*. 2015.

[16] Material Datasheet - Polypropylene Tatren RM 85 82 Clear https://molgroupchemicals.com/userfiles/products/80/80_tds_en.pdf Seen: 2024. Sept.

Intentionally blank

NOTIFICATION TO AUTHORS

The Journal MVM publishes original papers which have not been previously published in other journals. This is responsibility of the author. The authors agree that the copyright for their article is transferred to the publisher when the article is accepted for publication.

The language of the Journal is English.

Journal *Mobility & Vehicles Mechanics* is at the SSCI list.

All submitted manuscripts will be reviewed. Entire correspondence will be performed with the first-named author.

Authors will be notified of acceptance of their manuscripts, if their manuscripts are adopted.

INSTRUCTIONS TO AUTHORS AS REGARDS THE TECHNICAL ARRANGEMENTS OF MANUSCRIPTS:

Abstract is a separate Word document, "*First author family name_ABSTRACT.doc*". Native authors should write the abstract in both languages (Serbian and English). The abstracts of foreign authors will be translated in Serbian.

This document should include the following: 1) author's name, affiliation and title, the first named author's address and e-mail – for correspondence, 2) working title of the paper, 3) abstract containing no more then 100 words, 4) abstract containing no more than 5 key words.

The manuscript is the separate file, „*First author family name_Paper.doc*" which includes appendices and figures involved within the text. At the end of the paper, a reference list and eventual acknowledgements should be given. References to published literature should be quoted in the text brackets and grouped together at the end of the paper in numerical order.

Paper size: Max 16 pages of B5 format, excluding abstract
Text processor: Microsoft Word
Margins: left/right: mirror margin, inside: 2.5 cm, outside: 2 cm, top: 2.5 cm, bottom: 2 cm
Font: Times New Roman, 10 pt
Paper title: Uppercase, bold, 11 pt
Chapter title: Uppercase, bold, 10 pt
Subchapter title: Lowercase, bold, 10 pt
Table and chart width: max 125 mm
Figure and table title: Figure _ (Table _): Times New Roman, italic 10 pt

Manuscript submission: application should be sent to the following e-mail:

mvm@kg.ac.rs ; lukicj@kg.ac.rs
or posted to address of the Journal:
University of Kragujevac – Faculty of Engineering
International Journal M V M
Sestre Janjić 6, 34000 Kragujevac, Serbia

The Journal editorial board will send to the first-named author a copy of the Journal offprint.

OBAVEŠTENJE AUTORIMA

Časopis MVM objavljuje orginalne radove koji nisu prethodno objavljivani u drugim časopisima, što je odgovornost autora. Za rad koji je prihvaćen za štampu, prava umnožavanja pripadaju izdavaču.

Časopis se izdaje na engleskom jeziku.

Časopis *Mobility & Vehicles Mechanics* se nalazi na SSCI listi.

Svi prispeli radovi se recenziraju. Sva komunikacija se obavlja sa prvim autorom.

UPUTSTVO AUTORIMA ZA TEHNIČKU PRIPREMU RADOVA

Rezime je poseban Word dokument, "*First author family name_ABSTRACT.doc*". Za domaće autore je dvojezičan (srpski i engleski). Inostranim autorima rezime se prevodi na srpski jezik. Ovaj dokument treba da sadrži: 1) ime autora, zanimanje i zvanje, adresu prvog autora preko koje se obavlja sva potrebna korespondencija; 2) naslov rada; 3) kratak sažetak, do 100 reči, 4) do 5 ključnih reči.

Rad je poseban fajl, „*First author family name_Paper.doc*" koji sadrži priloge i slike uključene u tekst. Na kraju rada nalazi se spisak literature i eventualno zahvalnost. Numeraciju korišćenih referenci treba navesti u srednjim zagradama i grupisati ih na kraju rada po rastućem redosledu.

Dužina rada: Najviše 16 stranica B5 formata, ne uključujući rezime
Tekst procesor: Microsoft Word
Margine: levo/desno: mirror margine; unurašnja: 2.5 cm; spoljna: 2 cm, gore: 2.5 cm, dole: 2 cm
Font: Times New Roman, 10 pt
Naslov rada: Velika slova, bold, 11 pt
Naslov poglavlja: Velika slova, bold, 10 pt
Naslov potpoglavlja: Mala slova, bold, 10 pt
Širina tabela,dijagrama: max 125 mm
Nazivi slika, tabela: Figure __ (Table _): Times New Roman, italic 10 pt

Dostavljanje rada elektronski na E-mail: **mvm@kg.ac.rs ; lukicj@kg.ac.rs**

<div align="center">

ili poštom na adresu Časopisa
Redakcija časopisa M V M
Fakultet inženjerskih nauka
Sestre Janjić 6, 34000 Kragujevac, Srbija

</div>

Po objavljivanju rada, Redakcija časopisa šalje prvom autoru jedan primerak časopisa.